8-21-2012

Magneto-elastic behavior in hard- and soft-MRE's including demagnetizing effects

Juan Roche

MAGNETO-ELASTIC BEHAVIOR IN HARD- AND SOFT-MRE'S INCLUDING DEMAGNETIZING EFFECTS

by

Juan C. Roche

A Thesis

Submitted to the

Department of Mechanical Engineering

College of Engineering

In partial fulfillment of the requirement

For the degree of

Master of Science in Mechanical Engineering

at

Rowan University

June 18, 2012

Thesis Chair: Paris Von Lockette, Ph.D.

Thesis Committee:

TR Chandrupatla, PhD, Professor, Mechanical Engineering
Jennifer Kadlowec, PhD, Associate Professor, Mechanical Engineering
Samuel Lofland, PhD, Astronomy and Physics

Acknowledgements

I gratefully would like to acknowledge my advisor Dr. Paris Von Lockette for his insight and guidance throughout this thesis research project. I would like to express my sincere gratitude to Dr. Sam Lofland for his many valuable suggestions, encouragement, and assistance. I am also grateful to Dr. T.R. Chandrupatla and Dr. Jennifer Kadlowec for serving on my thesis committee.

Abstract

Juan C. Roche
MAGNETO-ELASTIC BEHAVIOR IN HARD- AND SOFT-MRE'S INCLUDING DEMAGNETIZING EFFECTS

This thesis studies the magnetic and mechanical behavior of magnetorheological elastomers (MREs) based on four possible permutations defined along particle alignment (Aligned and Unaligned) and magnetization (Hard- or Soft-magnetic) pairs. These pairs designations yield classes A-H, U-H, A-S and U-S. The last two classes comprise traditional MREs. Samples were fabricated by mixing DOW HS II silicone elastomer compound and 30% by volume of either nominally 40-micron M-type barium hexaferrite (BaM) or 325-mesh iron (Fe) particles cured with or without the presence of a magnetic field. Magnetization and density measurements were employed to help confirm fabrication of the four distinct classes. Results of magnetization measurements suggest that the goal of defining and fabricating the four classes was functionally achieved. The motivating for this project stems from the notion that in soft-magnetic particles (i.e. Fe), behavior is driven by local demagnetizing effects while hard-magnetic particles (i.e. BaM) have a preferred magnetic axis and therefore generate magnetic torques at the particle level. The larger thesis seeks to define, model, and differentiate the nature of the magnetic torque response across all four classes.

Table of Contents

Chapter 1: Introduction

1.1 Motivation

In this work, consideration is given to materials that consist of magnetically polarizable particles in a non-magnetic medium. These materials are commonly known as magnetorheological elastomers (MREs), Ginder *et al.* [1999]. MREs belong to the class of smart materials due to their ability to change their shear stiffness under the effect of a uniform field (e.g. Jolly *et al.* [1996] and Zhou [2003]). This thesis studies the magnetic and mechanical behavior of four classes of MRE composite materials consisting of magnetically hard and soft particles embedded firmly in a non-magnetic elastic matrix. The systematic study of the use of magnetically hard particles in MREs was a unique contribution to the field because traditionally, MREs are comprised of carbonyl iron particles which are magnetically soft and spherical.

The materials used experimentally in this thesis served as proxies for four theoretical alignment-magnetization symmetry classes of MREs along which material behavior was expected to diverge substantively. Alignment variation was constructed by either curing the material in an external magnetic field to align the particles or leaving particles unaligned (as mixed); in addition, either magnetically hard or soft particles were used to vary the composite's magnetization behavior. For a magnetically soft particle, behavior is driven by local demagnetizing effects while a magnetically hard particle has a

preferred magnetic axis and therefore generates magnetic torques at the particle level. The four classes are shown schematically in Figure 1.1.1

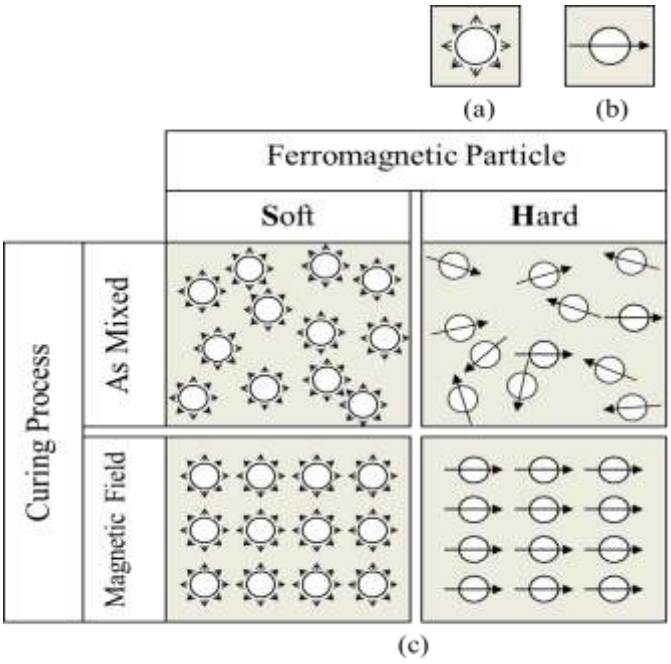

Figure 1.1.1 Iconography of (a) magnetically soft and (b) hard particles, and (c) schematics of four classes of MREs based on alignment during the curing process and either magnetically hard or soft particles.

In magnetically soft materials (Figure 1.1.2 (a)) the magnitude of the internal magnetization can be given as $m = \mu_o \mu_r H$. Furthermore, the magnetization vector M of the particles follows the applied magnetic field H, regardless of deformation (Figure 1.1.2 (b)). The magnetic torque density T within the particles themselves is determined by $T = M \times H$. Thus, there is no net torque acting on spherical (geometrically symmetric) particles within a uniform field if the composite is unperturbed with respect to that field since M and H are collinear. Furthermore, when chains of particles are sheared within the field, individual particle magnetizations still align with H (Figure 1.1.2 (b)); however,

demagnetizing effects between particles generate a restoring torque (or dipole moment) that seeks to minimize the energy of the system by returning particles to their unperturbed state, Shen *et al.* [2004].

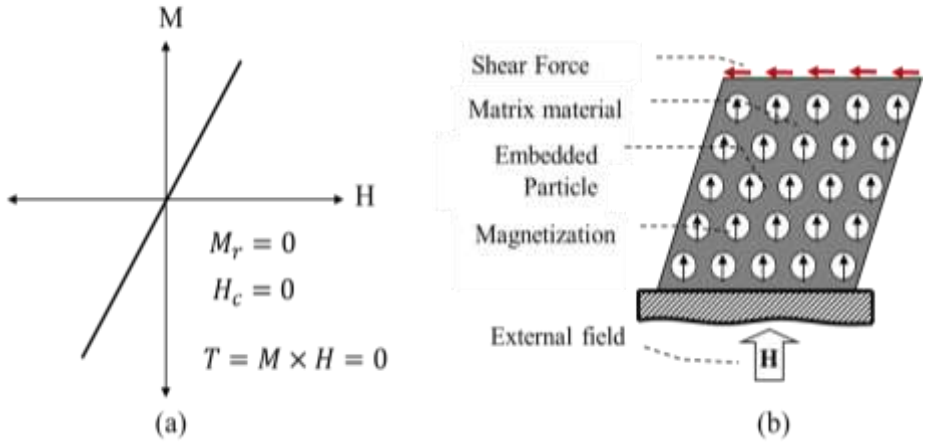

Figure 1.1.2 (a) Ideal, zero hysteresis, soft magnetic materials showing no remanent magnetization, M_r, and a zero coercive field value, H_c. (b) Effect of uniform field on S-MRE that uses aligned soft-magnetic particles under-shearing stress (red arrows). Particle magnetization M is shown in thin black arrows and local field H in block arrows.[1]

In an ideal hard magnetic material (Figure 1.1.3 (a)) the particles have a constant value of M when $H < |H_c|$. The fundamental difference between S-MRE and H-MREs lies in the torque generated by H within the embedded particles since M and H need not be collinear regardless of deformation (Figure 1.1.3 (b)). Consequently, in contrast to S-MREs with spherical particles, in the unperturbed state H-MREs can generate substantial

[1] Note: $M \parallel H$ are collinear, therefore $T = 0$, however demagnetization effects create local torques within particles with respect to the external field thereby causing a restoring torque in the bulk specimen. This results in experimentally measurable increases in stiffness seen in S-MREs.

torques. Thus, H-MREs can be more accurately described as *active* materials as opposed to reactive S-MREs.

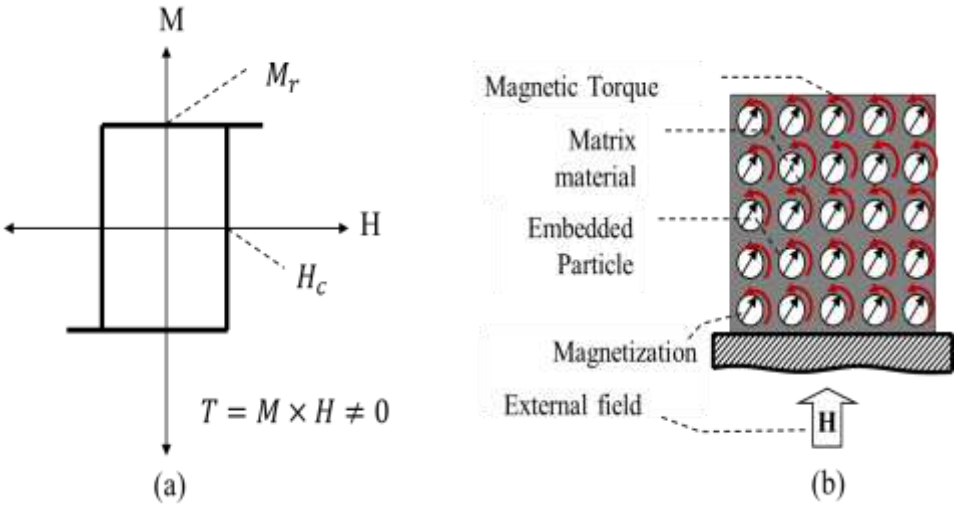

Figure 1.1.3 (a) Ideal hard magnetic material non-zero showing remanent magnetization and coercive field. The hysteresis curve is square. (b) Effect of uniform field on H-MRE that uses aligned hard-magnetic particles. Thin black arrows show the particle magnetizations M, block arrows show applied field H.[2]

Material proxy classes are defined along alignment (Aligned and Unaligned) magnetization (Hard- or Soft-magnetic) pairs generating four possible permutations. The magnetically hard particles lead to classes A-H and U-H, while the magnetically soft, provides classes A-S and U-S (i.e. traditional MREs). Classes A-H and A-S were aligned by an applied magnetic field of $\mu_0 H \sim 2$T prior to the curing of the matrix. The applied field induces dipole moments on the particles that ideally cause them, in materials with low volume fractions, to combine into extended, chain-like structures aligned with the

[2] Note: $M \nparallel H$ are not collinear, therefore $T \neq 0$. The torque within the particles produces a distributed internal moment within the composite that is resisted by the elastic stiffness of the matrix.

applied field, Jolly *et al*. [1996], Davis [1998], Yin and Sun [2005], and Boczkowska *et al.* [2009]. Classes U-H and U-S were not subject to a magnetic field during curing; thus, these materials are considered as unaligned and therefore spatially isotropic, Lokander and Stenberg [2003] and Gong *et al.* [2005]. The distinctions are important since the particle-field interactions for each class differ substantially, Wang *et al*. [2006].

The need for this study lies in the larger premise that the behaviors of classes A-S and U-S are driven primarily by demagnetizing effects while classes A-H and U-H are driven by torques produced in the particles. The goal of this chapter is to measure the magnetization of the samples to verify the development of the proxies for the four materials classes. The larger thesis seeks to define, model, and differentiate the nature of the magnetic torque response across all four classes. The methods used to complete these tasks are outlined below.

1.2 Methods

A vibrating sample magnetometer (VSM) was used to take measurements of the magnetization of the four cases. Measurements of the magnetization M component transverse as well as parallel to the poling field H in relation to the sample plane were attained. These measurements, detailed in Chapter 3, helped confirm fabrication of the four distinct classes.

A VSM was also used to study the orientation distribution of remanent magnetization in each material class. In preliminary experiments, especially for H-MREs, a hysteresis loop of M vs. H showed different values of the remanent magnetization M_r when measured parallel and perpendicular to the poling direction. This suggests a rotation of the ferromagnetic particles in the plane relative to H. To explore this possibility, we examined M_r while rotating the sample. Additionally, X-ray diffraction texture measurements were employed to assist the interpretation of particle distributions during the rotation. This work is detailed in Chapter 4.

Multiphysics finite element simulations with COMSOL were performed to validate development of computational models of MREs by comparing simulation results to experimental data. The cantilever bending actuation of samples with field was tested previously for all four classes, Von Lockette *et al*. [2011]. The combination of this cantilever bending experiment with magnetization measurements results helped with the development of a FEA model capable of predicting the coupled magneto-elastic behavior of the MREs. This work is detailed in Chapter 5. Finally, conclusions drawn from this study and the future directions of this project are summarized in Chapter 6.

Chapter 2: Literature Review

2.1 Experiments, Models, and Properties of MREs and the Effects of Compositional Parameters on their Properties

Literature selected herein provides a good foundation of what has been done and what has not in relation to the proposed work. Experiments and the effects of compositional parameters on their properties are examined. Moreover, previous mathematical, analytical, and computational models provide useful information to further the development of this thesis.

In the last few years, prompted largely by the work of Lord Corporation research group, numerous articles on the magneto-elastic behavior of MRE's have appeared. Jolly [1996] *et al.* created a model of the MR effect as a function of particle magnetization to measure the response of the composite to a magnetic field. The model established a mechanism by which magnetic flux density is distributed within the composite material accounting for nonlinearities and saturation. The maximum field-induced change in stress occurred when the particles became magnetically saturated. In their model, there was a noticeable discrepancy between theory and experimental results. Therefore, a parameter to adjust experimental data to the model was needed. This parameter accounted for un-modeled magnetic interactions, such as demagnetizing effects.

Davis' [1999] model provides a mathematical description of the rubber matrix properties leading to an expression for the effect of volume fraction of iron (Fe) particles

on shear modulus as a function of H. They consider the high-field limit and calculate the maximum change in shear modulus due to H. In this model, Fe particles are treated as rigid spherical shells in a continuous matrix. The magnetic properties of the particles were represented by a nonlinear magnetic induction B as a function of H. This relationship becomes $B = \mu H$ at small magnetic fields and $B = \mu_0(H + M_s)$ above saturation. Where μ is the permeability of the filler particle (e.g. Fe), $\mu_0 = 4\pi x 10^{-7}$ H/ m, and M_s is the saturation magnetization of the filler particles. Typical values for Fe are $\mu = 1000\mu_0$ and $\mu_0 M_s = 2$T. The mechanical response is described in terms of the principal extension ratios λ_i, which are the ratios of the current length (deformed) to original (non-deformed) length in the principal directions. Incompressibility is assumed, so that for any deformation $\lambda_1\lambda_2\lambda_3 = 1$. The shear modulus at zero magnetic fields for the sample with aligned particles is less than that for the sample with randomly dispersed particles at the same volume fraction. The optimum volume fraction of the particles is predicted to be 27%. This is important because it is desirable to have the ratio of the magnetically induced change in shear modulus to be as large as possible.

Ginder [2002] *et al.* reported preliminary measurements of the field-induced increase in dynamic modulus and length change on MREs. To study the dynamic shear modulus they built a tuned vibration absorber (TVA). The device was clearly tunable by a magnetic field, with a resonance that shifted upward in frequency by over 20% at 0.56 T. The transmissibility was found to decrease as the amplitude of the base acceleration increased. From the measure of transmissibility and phase, the dynamic spring rate was calculated. Furthermore, they built a lever-arm-based dilatometer to allow measurements

of the length changes in cylindrical MRE's. They noted that by attaching masses to the lever arm the effect of compressive preload on the length change could also be studied. Obviously, the magnitude of the magnetostriction (i.e. length change) of the sample was greater than that obtained in bulk Fe. They argued that this result was due to inter-particle or shape effects.

Zhou [2003] tested the damped free vibration of an MRE spring and mass system. Zhou determined the shear properties and damping factor by calculating the dependence of the natural frequency and damping ratio of the system on the applied field. The commonly used point-dipole model was not suitable in this experiment when the shear modulus was linear in H, as found for small fields. In addition, the local saturation of the particles was considered since the natural frequency is affected by the magnetic force between the particles inside the matrix. The total magnetic energy density was used to analyze the shear stress induced by inter-particle magnetic forces. By taking the derivative of the total magnetic energy density with respect to the relative position of two adjacent particles in a chain after deformation (when the magnetic field is applied along the z direction) the stress induced can be computed and the damping factor was shown to be independent of the applied field.

Zhou and Li [2003] tested the accelerations of an MRE and cuprous mass system under (uniaxial) displacement excitation. The generation of hysteresis loops was highly noticeable through the paper. They employed this method to describe the change of the system with applied magnetic field and exciting frequency under harmonic excitation.

They argue that the method is a useful tool when showing the dynamic behavior of a system. Some of the characteristics of the system examined were the energy dissipated per cycle, identification of a linear vs. nonlinear system behavior, phase delay between the excitation and the response for a linear system. They showed that the mechanical behavior was nonlinear and the field-dependent behavior of the MRE was associated with the applied frequency. However, they acknowledged the existence of eddy current damping from the brass mass that added to energy loss in the system, which is not directly dependent on the MRE material.

Lokander and Stenberg [2003] produced and investigated isotropic MR solids made of nitrile rubber (with various acrylonitrile contents) and two different types of iron particles: large, irregularly shaped iron particles and spherical carbonyl iron powders. They discovered that the MR effect of irregularly shaped iron particles is larger compared to the carbonyl iron powders. A maximum occurs at a particle content of about 30% by volume and size > 60 μm of the irregularly shaped particles. They found that isotropic MREs materials with irregularly shaped particles show an increase in modulus of about 0.4 MPa, while aligned MREs with carbonyl iron show an increase of 0.7 MPa. In addition, they found that the absolute MR effect could be improved by the addition of plasticizers or by using a softer matrix material, such as silicone rubber.

Zhou and Jiang [2004] presented the real-time dynamic deformation progress using a white light speckle technique for deformation analysis of MREs and elastomer-ferromagnet composites (EFCs). In this case, the MREs were cured under a strong

magnetic field while the EFCs were not (i.e. the ferrous particles are embedded randomly in the matrix). Therefore the mechanical properties of these two kinds of materials were very different. The white light speckle technique consisted of the retrieval of the in-plane displacement of the sample from a series of images recording the speckle pattern during deformation. The speckle movement calculated by the intensity correlation of consequent images was related to the displacement distribution on the surface of the sample. As a result, by calculating the correlation of a series of recorded images numerically, they obtained the in-plane displacement of a sample at different times. Based on this study they concluded that the deformation of the samples driven by magnetic field is related to the field strength. The MREs were compressed along the direction of the applied magnetic field while EFCs is dilated. The deformation of the MREs changes slightly with volume fraction and is smaller than that of EFCs. Thus, the MRE was stiffer than the EFCs in the direction of the chain-like structures formed in MREs cured in the presence of a magnetic field.

Zhou [2004] presented a different data processing method to recover the shear modulus of an MRE in the frequency domain through the measured force excitation and acceleration response of the mass in the aforementioned experiment (Zhou and Li [2003]), based on the Steiglitz-McBride [1965] interaction method. An analysis of the recovered shear modulus was performed in three ranges of the frequency domain (i.e. low, moderate, and high). In the low-frequency range the average shear modulus changes proportionally with the magnetic field until magnetic saturation occurs. The maximum relative change in shear modulus was 55%.. They argue that in the moderate-frequency

range and high-frequency range, the shear modulus was too complex to be analyzed by their proposed method.

Gong *et al*. [2005] investigated the effects of carbonyl iron particles and additives (*e.g.* silicone oil and rubber) on the MR effect and the relationship between microstructure and mechanical properties. They found that, due to the help of the silicone oil, MREs contain a self-assembled microstructure of particles. Under the magnetic field, the particles become magnetized and move slightly, due to the lubrication action of the oil, to form a regular structure, which result in a high MR effect. The best MR effect was obtained for a sample with 60% of carbonyl iron particles, 20% of silicone rubber and 20% silicone oil. The elastic modulus enhancement reached 60%, which represent the same degree as for the anisotropic MR elastomers fabricated under a strong magnetic field. Furthermore, they proposed a simple micro-assemble model to explain the MR effect, which was in agreement with the results.

Yin and Sun [2005] investigated the particle interaction forces and elastic distributions in both the particles and the matrix phases of a composite subject to both magnetic and mechanical loading. Magnetic interaction forces were induced by the large relative magnetic permeability of the particles (as high as 10^2 to 10^5 times the relative permeability of the matrix). Since their model involves a transverse isotropic symmetry, they argue that by applying a uniaxial loading and shear load in the plane normal to the direction of the expected chain structures, the Young's modulus can be calculated. They found that the model has a quadratic prediction of the elastic response at high-applied

magnetic field and a linear tendency when the applied flux density is small. They argue that this difference is a result of nonlinear magnetizing behavior of the particles and demagnetizing field effect during the fabrication and experiments. They show that there exists an optimal particle volume fraction to maximize magneto-elasticity. Although they do not give a value, they argued that is because volume fractions of 10% and 20% yield similar shear modulus results before magnetization becomes saturated. Their predictions suggest that the higher the volume fraction, the higher the saturation flux density. Iron composites of 10%, 20%, and 30% were saturated at 0.55, 0.72, and 0.88 T, respectively.

Vargas *et al.* [2006] established the effect of the external magnetic field on the elastic modulus. They determined the elastic modulus of isotropic and anisotropic magnetic elastomers using five different experimental set-ups (see Figure 2.1.1) depending on the direction of the magnetic field, particle alignment, and mechanical stress. They have found that anisotropic magnetic elastomers exhibit much larger increase in modulus than the isotropic ones. In addition, their mechanical properties (i.e. elastic modulus and stress–strain behavior) are significantly different when characterized parallel and perpendicular to the particle alignment. The most significant result (i.e. the change in modulus) was found in anisotropic magnetic elastomers if the applied field, the particle alignment, and the mechanical stress are all parallel with respect to each other.

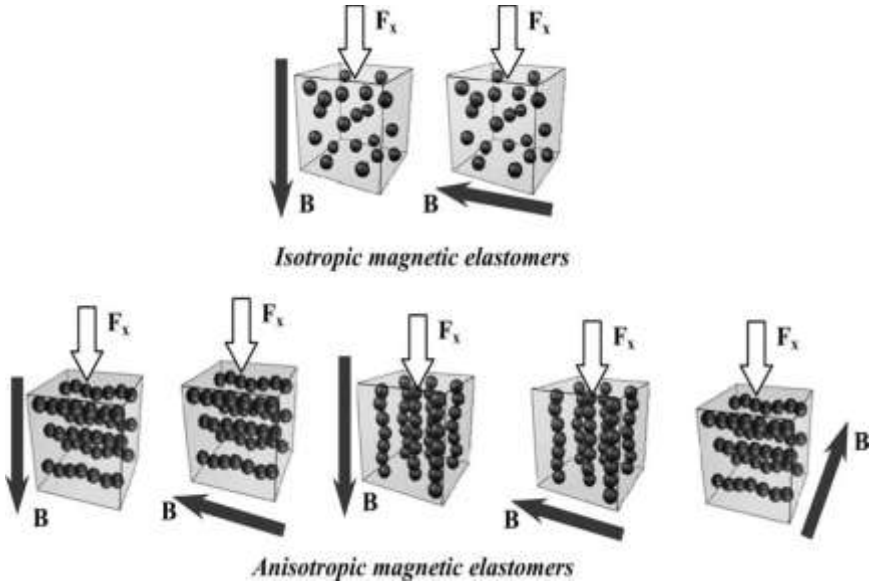

Figure 2.1.1 Experimental set-ups proposed by Vargas *et al.* [2006]. White arrow indicates the direction of the force and black arrow shows the direction of magnetic field.

Wang [2006] *et al.* studied the influence of interactions between particles and matrix on the performance of MRE's, including the change of shear modulus and mechanical properties. In their study, modifications of the matrix/particle interactions were controlled by using different kinds of silane coupling agents (i.e. AH-151 and KH-550). The addition of the silane agents improved the dispersion of the particles and the adhesion between the particles and matrix. These modifications led to an improvement of the composite mechanical properties. The tensile strength of the composites with silane coupling agents AH-151 and KH-550 increased by 77% and 62%, respectively. Thus, an effective method to improve the mechanical properties of MREs is to control the matrix/particle interactions. AH-151 improved the relative MR effect by 37% under a magnetic field of 0.6 mT. Conversely, KH-550 decreased both relative and absolute MR effect.

2.2 Continuum Mechanics and Magneto-Elastic Coupling

There are two different approaches to the study of the magneto elasticity of MREs: firstly, theories that treat the problem from the viewpoint of continuum mechanics, which formally couple elasticity and electromagnetic field theories on various arrangements of particles, and secondly, energy-based theories that attempt to derive magneto-elastic properties from idealized models of the structure of the particulate composite. Consequently, there are several works in the literature that present the full system of equations suitable for the magneto-elastic deformation of MREs.

Borcea and Bruno [2001] calculated the distribution of magnetization in MR solid composites from the basic minimum energy principle of magneto-elasticity, taking into account the fully coupled magneto-elastic interactions. They considered random, statistically homogeneous distributions of ferromagnetic inclusions (diameter $\geq 1.5\,\mu$m) within an elastic matrix and evaluated the overall properties in the regime in which the volume fraction of particles is small. They argue that their approximation is justified for cubic crystalline ferromagnetic materials, such as iron and iron–cobalt alloys and for polycrystalline particles. For ferromagnetic particles that satisfy the above assumptions, their method of solution is valid. For real systems, both the anisotropy effects and the existence of varying magnetizations within the particles must be taken into account. Their calculations were made under the assumption that the ferromagnetic particles were uniformly magnetized when the material had been cured in magnetic field.

The Yin [2002] *et al.* micromechanics based model investigated the microstructure of particle-filled composites subject to both magnetic and mechanical loading derived from strain energy functions. They considered a two-phase isotropic composite consisting of an elastomer matrix and ferromagnetic spherical particles. They evaluated the effective free energy in the magnetostrictive composite and presented numerical results and comparisons based on their method. To demonstrate the capability of their model they considered the case of uniaxial stress loading of the composites with a saturated magnetostriction. They considered the strain energies from both the particles and the matrix. The model also predicted the nonlinear finite deformation behavior of the composites. In their proposed method, it is noticeable that the mechanical uniaxial loading direction was the same as the saturated magnetic field. The volume fraction of the particles had a significant effect on the hyperelastic response (i.e. stress vs. stretch curves) of the composite. They argued that if the volume fraction of the particles is large the strain energy in the particles should be considered. Many models ignore the contribution of the strain energy from the particles. Although, they have included the local deformation mechanism of interacting particles in their model, they ignored the magnetic dipole interactions between particles. Including these effects on the modeling of such composites may have improved their results.

Dorfman and Ogden [2003] presented a summary of the relevant continuum mechanics equations and general theory that governs the deformation of magneto-sensitive elastic solids. In particular, they examined constitutive relations for isotropic magneto-sensitive solids. To demonstrate the application of the constitutive model and

theory they considered a sample confined to a circular cylindrical tube in the presence of a radial magnetic field and subject to a transverse shearing deformation. Two specific models were studied. First, they considered strain energy as a function of shear stress. In this case, the relationship between shear stress and displacement is linear. They found that as the magnetic field strength increases a given displacement requires a larger value of the shear stress to maintain mechanical equilibrium. Thus, the response of the device becomes stiffer. In the second study, they consider a strain-energy function that led to a nonlinear relationship between shear stress and displacement. They found that for a given displacement the required shear stress increases with the magnetic field strength. From these two models, they have concluded that the effect of the magnetic field is to stiffen the shear response of the material.

The model of Shen *et al.* [2004] consisted of a modified Ogden [1984] model that represented a nonlinear stress-strain relationship as well as all the dipole interactions in a MRE composite assumed to contain parallel chains of particles. They showed that the shear modulus change was quadratically proportional to the value of dipole moment. This modulus change was highly affected by the ratio of mean distance between two adjacent particles to the mean radius of the particles. Theoretical results were a good representation of the stress-strain relationship when compared to experimental results. However, a discrepancy was noticeable in the comparison. In the model, the mean distance between two particles was treated as constant during deformation and the interaction between chains has been neglected. These two factors may explain the discrepancy between the model and test data.

Kankanala and Triantafyllidis [2004] presented two different approaches to the continuum formulations for MREs, with negligible dissipative and hysteretic behavior. First, they present a direct approach based on the second law of thermodynamics and the conservation laws of mechanics. Secondly, a novel energy approach based on the unconstrained minimization of a potential energy functional is offered. They revealed that both approaches yielded the same governing equations and boundary conditions. To illustrate the magneto-elastic coupling phenomena they used a free energy function for a magnetorheological elastomer with cylindrical shape, subjected to traction or torsion, under the presence of external magnetic field.

Although the aforementioned models provide important guidelines to simulate such behavior, most of their solutions are idealized in the sense that they apply only to bodies of infinite extent and derived for isotropic magneto-elastic materials. Recently, Tuan and Marvalova [2010] adopted the formulation of Dorfmann and Ogden [2004,2005] and summarized the relevant magnetic and mechanical balance equations, boundary conditions, and general constitutive equations for magneto-elastic interactions for both compressible and incompressible magneto-elastic materials and then used them for specific application to incompressible, anisotropic magneto-elastic materials. They presented the simulation of the simple shear of a rectangular block of finite size subjected to a magnetic field, which, in the far field, is uniform and perpendicular to the shear direction. The constitutive equations are based on a modified free-energy function that

depends, in addition to the deformation gradient, on the magnetic flux density vector as the independent magnetic variable.

Castañeda and Galipeau [2010, 2011] address the important problem of non-spherical particles in an MRE composite. The work is important since particle asymmetry is the only way to develop magnetic anisotropy in soft-magnetic materials such as Fe. It is this magnetic anisotropy and the torques generated at the particle level that break magnetic symmetry and open new classes of material behavior. The 2011 work solves the problem of arbitrarily shaped, soft-magnetic uniformly oriented ellipses subjected to a magnetic field collinear with the major axis of the ellipse. The work finds that magnetostriction is a complex function of particle aspect ratio and volume fraction.

2.3 Summary

Prior works on MREs, theoretical and experimental, have almost exclusively dealt with roughly spherical soft-magnetic filler particles, i.e. carbonyl iron (see Table 2.3.1) whereas this work seeks to address the use of hard-magnetic filler particles. The critical difference stems from the development of torques at the particle level which occurs in hard-magnetic materials. Though magnetic torques may occur in soft-magnetic materials having some shape anisotropy, this additionally requires that the shape anisotropy is not collinear with the external field, which has not been addressed in the literature.

Table 2.3.1: A sampling of constituent use in the MRE literature[3]

particle type	particle size	particle volume fraction (%)	matrix	used in
silicon steel alnico alloy	0.15 - 0.20 mm	0.3, 0.5, 0.7	silicone rubber	Bednarek (2000)
carbonyl iron	~ 3 μm	~0.27	natural rubber or cis-poly(isoprene)	Ginder, *et al.* (2002)
carbonyl iron	3 μm	0.27	silicone rubber	Zhou and Li (2003)
carbonyl iron iron	3.9 – 5 μm < 60 μm	0 - 0.5	nitrile rubber natural rubber	Lokander and Stenberg (2003)
carbonyl iron	3 μm	0.2 – 0.7	silicone rubber	Gong, *et al*. (2005)
carbonyl iron iron oxide	2.5 μm	0.1 – 0.3	poly(dimethyl siloxane)	Varga, *et al*. (2005-2006)
carbonyl iron	3-5 μm	-	polyurethane/Si-rubber	Hu, *et al.* (2005)
carbonyl iron	3-5 μm	-	silicone rubber /Polystyrene	Wang, *et al*. (2006-2007)
carbonyl iron	3-11 μm	0.6	natural rubber silicone rubber	Chen, *et al*. (2007)
Iron	10-40 μm	0 – 0.3	silicone rubber	Von Lockette, *et al*. (2008)
carbonyl iron	3.5 μm	0.3	natural rubber	Jiang, *et al*. (2008)
iron BaM	40 μm	0.3	silicone rubber	Von Lockette, *et al.* (2009-2011)

[3] In addition to the actual matrix, additives like oils and other mixing agents are normally used in synthesis. The behavior of MREs depends fundamentally on the characteristics of the composite materials (i.e. there exist many compositional parameters that influence this characteristic behavior, including but not limited to: the matrix and filler particles of the composite; the shape, volume fraction, and distribution of the particles and whether the composite is un-poled or pole during the curing process).

The focus of theoretical derivation has been to estimate improvements to shear modulus or to predict enhancements to shear-driven responses. Experimental work has also largely focused on shearing behavior with a notable exception examining compression, but these works based shear response on magnetostrictive phenomena – magnetic field affecting changes in inter-particle spacing – and have not dealt with torque driven behavior which is the focus of this thesis.

Chapter 3: Fabrication and Validation of Proxies for Four Magnetic Symmetry Classes

3.1 Fabrication of MRE Composites

Samples were fabricated by mixing DOW HS II silicone elastomer compound and 30% by volume of either nominally 40 micron M-type barium hexaferrite (BaM) or 325-mesh iron (Fe) particles. All particles were nominally spherical. MRE materials made with BaM and Fe powders, aligned and unaligned, served as proxies for each of the four classes in this work. In order to validate their fabrication we used the following methods.

3.2 Density Measurements

In order to confirm the magnetic particle volume content, or volume fraction, of the samples (a characteristic important to the elasto-magnetic performance), the density of each sample was measured following Lokander and Stenberg [2003]. This constitutes an important check since the highest MR effect has been found to occur between volume fractions of 27% to 30% by numerical means (e.g. Davis [1998]) and with experiment (e.g. Demchuk and Kuzmin [2002]).

The measured densities of each sample are shown in Table 3.2.1. The density values were determined experimentally by measuring the mass of the samples in air and

then submerging them into a container (known volume) filled with water (known density). The submerged sample experiences a buoyant force equal to the volume of the displace water, allowing calculation of the samples density via the Archimedes' principle

$$\rho_s = \frac{m_s}{(m_s - m_{df})}\rho_w \tag{3.2.1}$$

where m_s is the mass of the sample in air, m_{df} the mass of the displace water, $\rho_w = 1\ \mathrm{g/cm^3}$ the density of water, and ρ_s the density of the sample. Once the density of the composite is obtained, the particle volume fraction c_p of the sample can be calculated by

$$c_p = \frac{\rho_s - \rho_{rubber}}{\rho_p - \rho_{rubber}} \tag{3.2.2}$$

where $\rho_{rubber} = 1.21\ \mathrm{g/cm^3}$ is the density of the rubber and ρ_p the density of the filler particle (for BaM, $5.27\ \mathrm{g/cm^3}$ and for Fe, $7.87\ \mathrm{g/cm^3}$).

Table 3.2.1 Summary of results obtained from density measurements. Calculated volume fractions are within desirable values.

Class	**Density** $\boldsymbol{\rho_s}$ **(g/cm³)**	**Volume fraction** $\boldsymbol{c_p}$(%)
A-S	3.41	33
U-S	3.24	30
A-H	2.42	30
U-H	2.70	36

3.3 Magnetization Measurements

The magnetization of H-MREs and S-MREs was measured with a VSM in fields up to $\mu_o H = 1.7$ T in order to verify the generation of proxies for the four classifications of materials. Measurements were done parallel (along the so-called easy axis) and perpendicular (along the so-called hard axis) to the alignment axis. Magnetization M is defined as a measure of the magnetic moment m_i per unit volume V of the sample or

$$M = \sum_i \frac{m_i}{V} \tag{3.3.1}$$

The internal magnetic field is the superposition of the applied magnetic field and the magnetic field created by the material itself (i.e. the magnetic field caused by the dipole moment of all the particles which is the demagnetizing field), that is expressed by

$$H_{in} = H_{app} + H_D \tag{3.3.2}$$

where H_{in}, H_{app}, and H_D are respectively the internal, the applied and the demagnetizing magnetic field. The intensity of the demagnetization field is linearly related to the magnetization by a geometry dependent constant called the demagnetizing factor N, so that we have

$$H_D = -N4\pi M \tag{3.3.3}$$

Since the experiment was carried out on cylindrical samples ~6 mm tall and 5 mm in diameter $N = 1/3$, Chikazumi [1997]. The internal magnetic field including the demagnetizing factor is then defined by

$$H_{in} = H_{app} - \frac{4\pi}{3} M \tag{3.3.4}$$

From a $M\ vs\ H$ curve, a number of magnetic properties can be determined. For example, when a magnetic material is exposed to a sufficient field the magnetization reaches a saturation point, i.e. saturation magnetization, M_s. When H is reversed M returns to zero at the coercive field H_c. BaM with coercive field $\mu_0 H_c > 0.4$ T provided the hard-magnetic behavior while Fe $\mu_0 H_c < 2.5$ mT, served as the soft magnet. Material classes A-H and A-S were produced by curing in $\mu_0 H \sim 2$ T to produce anisotropy in particle alignments while material classes U-H and U-S were cured as mixed in ambient field. Magnetic anisotropy especially in the case of hard-magnetic materials produces remanent magnetization M_r, which remains even when $H = 0$.

Figure 3.3.1 shows the magnetization cycle for the A-H sample. The data show a relatively constant value of the magnetization, outside of the hysteretic regions, when measured in the parallel direction. Most notably, the differences in quantities such as the H_c and M_r when measure in different directions. For example a lower coercive field is observed when measure in the perpendicular direction with respect to the poling direction. This suggests that relatively, a smaller applied magnetic field is required to reverse magnetization in the perpendicular direction, a 60% reduction from the parallel

direction. An important result is that ideally, in the aligned cases the remanent magnetization should be zero perpendicular to the alignment axis. However, results showing non-zero remanent magnetization (a 73% decrease from the parallel direction) suggest otherwise. Clearly this suggests a rotation of the ferromagnetic particles in the plane relative to the applied field. Therefore, the need for a better understanding of this phenomenon is necessary.

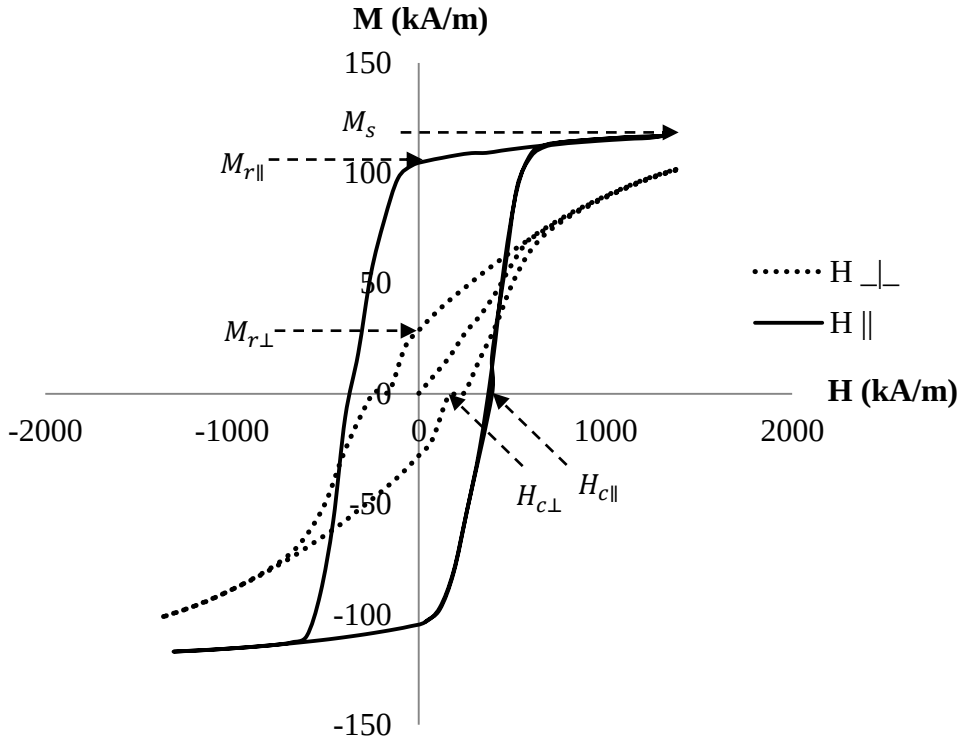

Figure 3.3.1: Magnetization cycles, M versus H, for the A-H material perpendicular and parallel to the alignment axis of the sample. The graphs show remarkable difference in quantities such as the coercive field H_c and remanent magnetization M_r when measure in different directions. The dashed line is the hysteresis loop when H is along the hard axis.

Figure 3.3.2 shows the results of a type U-H (H-MRE) material. The magnetization clearly increases with increasing field strength similarly to the A-H

material when measured in the perpendicular direction with respect to the main axis of the sample. Remanent magnetization for the material shows $M_r = 61\ \mathrm{kA/m}$ resulting from the hard-magnetic particles a reduction of 54.1% from A-H case which was expected due to lack of initial order. However, in contrast to the A-H material, the U-H material shows equivalence in $M\ vs\ H$ in other directions suggesting bulk isotropy (i.e. unaligned in the bulk).

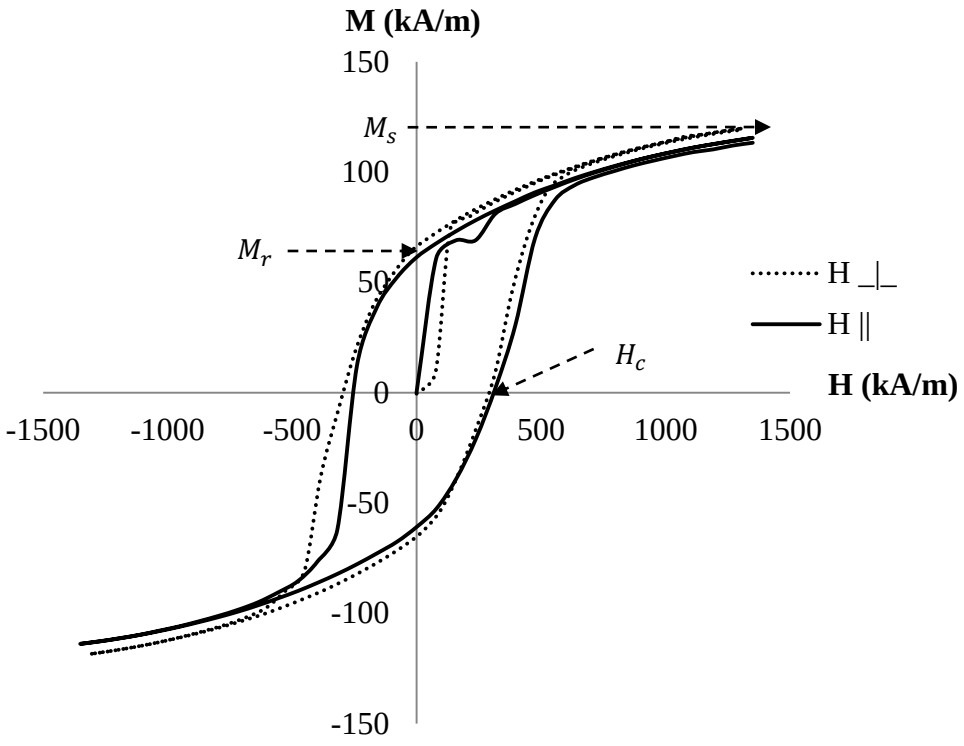

Figure 3.3.2: U-H magnetization curves, *M* versus *H*. In contrast to the A-H material, the U-H material shows equivalence in $M\ vs\ H$ in other directions. The dashed line is the hysteresis loop when H is along the hard axis.

Figure 3.3.3 shows the S-MRE type A-S material. As expected, result show no M_r and an initially linear behavior until the magnetization begins to saturate. The saturation magnetization of the composite was found to be $M_s = 640\ \mathrm{kA/m}$.

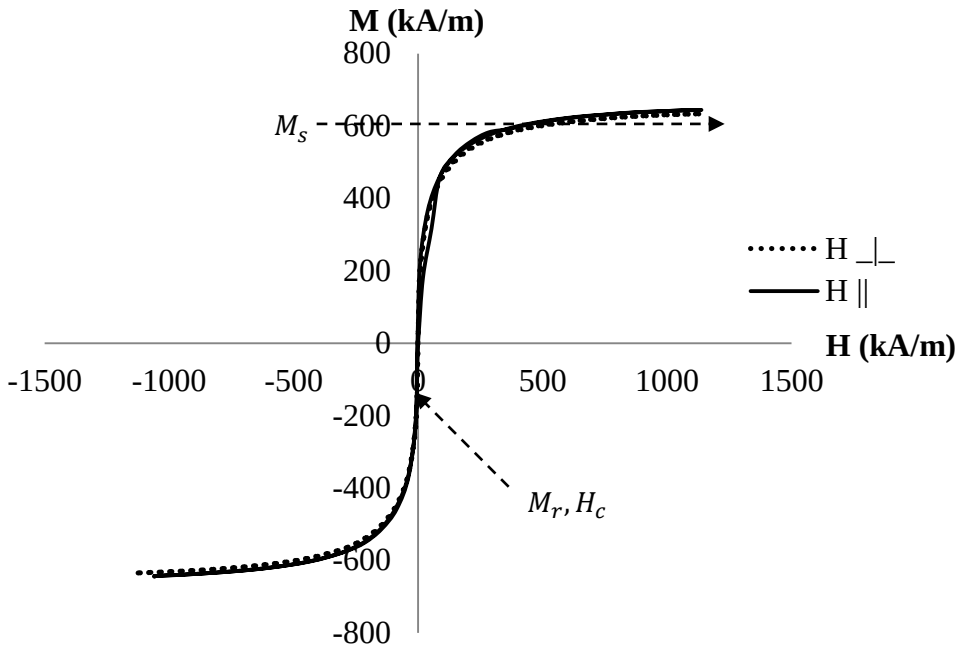

Figure 3.3.3: A-S magnetization curves, M versus H. The results show negligible difference in quantities such as the coercive field H_c and remanent magnetization M_r when measured in other directions.

Figure 3.3.4 shows the S-MRE type U-S material's magnetic behavior. As expected, result show $M_r = 0$, and an initially linear behavior until the magnetization begins to saturate, which saturates at $M_s = 570\ \mathrm{kA/m}$. If we compare the S-MREs behavior we found that is uniform in orthogonal directions. While this is expected for the unaligned case, where the particle are assumed left randomly arranged as mixed, it is surprising for the aligned case – but can likely be expected at large volume fractions

since particles are no longer free to move. Their behavior in general is in line with traditional MREs.

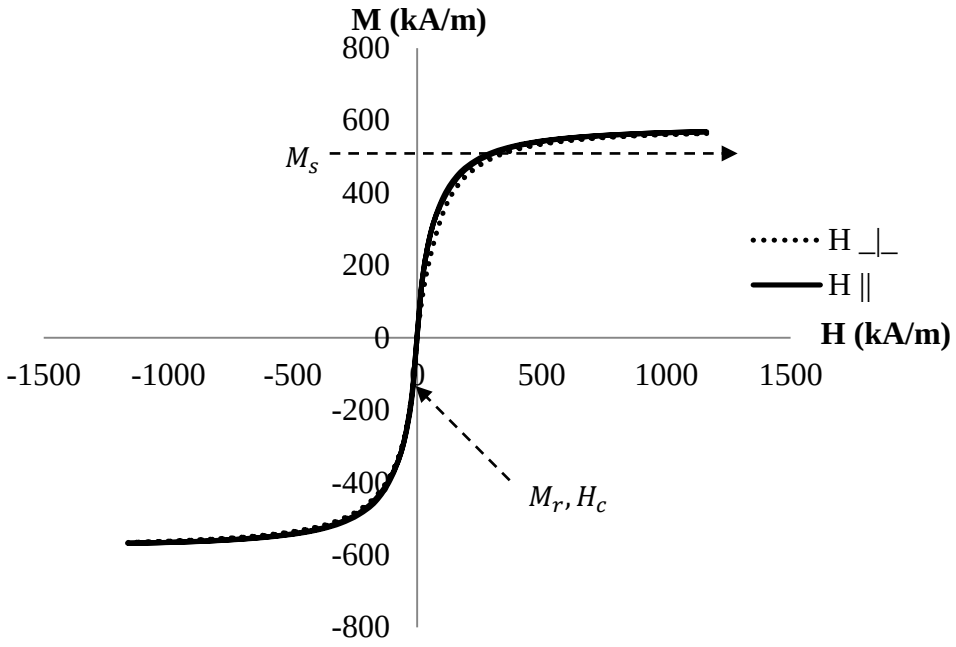

Figure 3.3.4: U-S magnetization curves, M vs. H.

From the knowledge of both the saturation magnetization of the ferromagnetic material (i.e. the filler particle) and of the sample, the particle volume fraction f can be calculated in an alternate fashion. The particle volume fraction of the sample was calculated with

$$f = \frac{M_s}{M_{sp}} \times 100, \qquad (3.3.5)$$

where M_s is the saturation magnetization of the sample and M_{sp} of the filler particle. Results show values between 30%-36% across all samples, in agreement with the density measurement suggesting that there are a) very few voids and b) the particles maintain their magnetic properties.

Table 3.3.1: Physical and magnetic properties of H- and S-MREs classes and materials investigated.

Class	Density ρ_{tot} (g/cc)	Saturation Magnetization M_s (kA/m)	Remanent Magnetization M_r(kA/m)	Coercive Field H_c (kA/m)	Volume fraction c_p(%) eq.(3.2.2)	Volume fraction f (%) eq. (3.3.5)
A-H	2.42	120	∥103, ⊥ 28	∥394, ⊥ 158	30	30
U-H	2.70	141	61	318	36	35
A-S	3.41	640	0	0.36	33	36
U-S	3.24	570	0	1	30	32

Material	Density ρ_p (g/cc)	Saturation magnetization M_{sp} (kA/m)	Coercive Field H_c (kA/m)
BaM	5.27	400	> 300
Fe	7.87	1800	<2
rubber	1.21	0	0

3.4 Conclusion

Results of magnetization measurements suggest that the goal of defining and fabricating four symmetry classes (based on alignment-magnetization pairs) of MRE materials has been functionally achieved. For example, the fact that calculated $M_r = 0$ in both S-MREs cases and is non-zero in both H-MRE cases verifies differentiation of the soft- *vs.* hard-magnetic behaviors. Results show that A-H, aligned H-MRE material, exhibit differential remanent magnetizations and coercive fields along the parallel (aligned) and perpendicular axes, further validating differentiation due to alignment during curing.[4] In addition, a number of magnetic properties of the studied materials were determined. Also measurements of the saturation magnetization yielded volume fractions values similar to the ones obtain by using the Archimedes principle which indicates that all samples contain few air pockets and the particles maintain their magnetic properties.

[4] Ideally, in the aligned cases remanent magnetization would be zero perpendicular to the alignment axis. However, results showing non-zero remanent magnetization in the A-H material perpendicular to the alignment axis suggest otherwise. To better understand the orientation of particle magnetizations, a distribution model for the interpretation of particle alignments in H-MRE's is presented in the next chapter.

Chapter 4: Modeling Distribution of Magnetization in A-H

4.1 Remanent Magnetization Study

Remanent magnetization M_r is the magnetization left behind in the samples after the applied magnetic field is removed. We measured M_r as a function of orientation with respect to the alignment (or curing) axis. The experiment was carried out at room temperature on samples ~6mm tall and ~5mm in diameter cut from larger specimens of 25 mm square. Samples were studied with the same VSM system used to study M_s and H_c (see Chapter 3). A sample was mounted such that it could be turned about its geometric axis in a fixed magnetic field. To begin, the sample was placed in a magnetic saturation state by a $\mu_o H_{app} = 1.6\,\mathrm{T}$ field, then H_{app} was set to zero and M_r was measured. Next, the sample was rotated by a 5° increment and the process repeated through 90°. The results are presented in Figure 4.1.1

In previous experiment (using a different sample cut from the sample bulk material), a hysteresis loop of M vs. H, showed $M_{r\parallel} = 103$ and $M_{r\perp} = 28$ kA/m, parallel and perpendicular to the poling direction, respectively (see previous Chapter). This suggests a rotation of the ferromagnetic particles in the plane relative to the applied field.

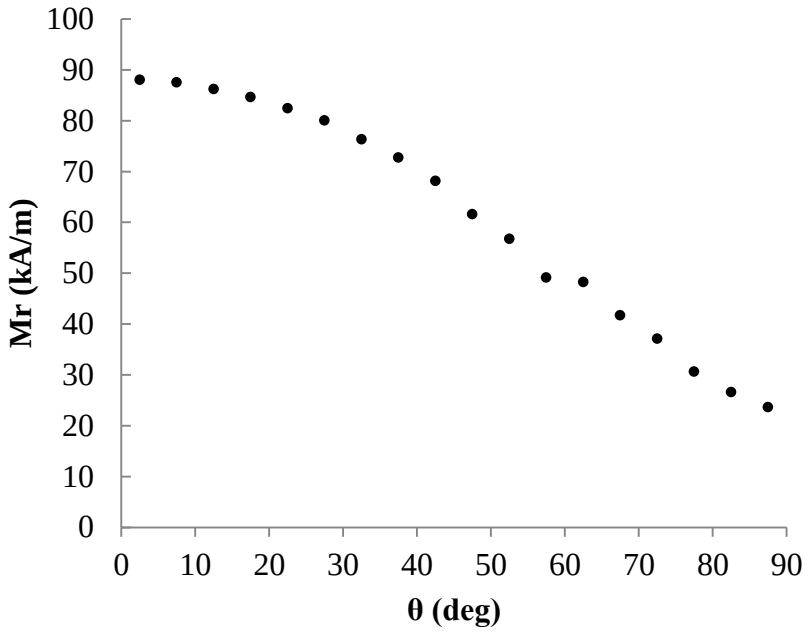

Figure 4.1.1 Results of M_r as a function of orientation θ where the alignment direction is $\theta = 0$ and one observes a maximum there, as expected.

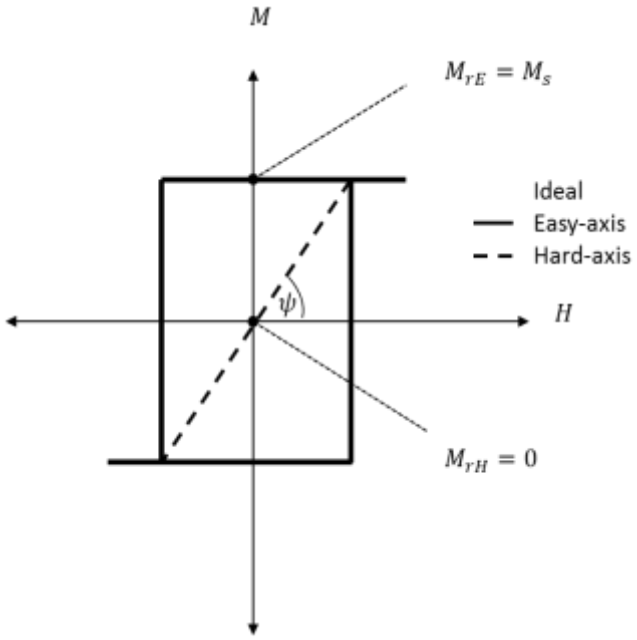

Figure 4.1.2 Ideal magnetization curves along hard-axis (in-plane) and easy-axis (perpendicular), where M_{rE} and M_{rH}, are the remanent magnetizations on the easy and hard axes respectively.

One-way to understand the underlying phenomenon is to look at the ratio M_r/M_s called squareness, Jiles [1998]. When this ratio is close to unity, H is close to some orientation defined as the easy-axis and the hysteresis loop is closest to a square shape (e.g. $M_r/M_s = 0.86$ for A-H when measured in parallel to the poling axis, see previous Chapter Figure 3.3.1). The angle the magnetic field makes with the easy-axis (say ψ) can be increased (by rotating the sample in plane) and the opening of the hysteresis loop is reduced; it is largest when H is parallel to the easy-axis and smallest when H is parallel to the so called hard-axis.

4.2 XRD-Texture Study

The orientation distribution of the particles (in H-MREs) was explored by X-ray diffraction texture measurements. A material is textured if the particles are aligned in a preferred orientation along a certain direction (e.g. in class A-H). The "texture" is usually introduced in the fabrication process (e.g. by applying a magnetic field during curing) and affects the material properties by introducing structural anisotropy. The texture analysis determines the preferred orientation of the crystallites within the sample. It is possible to determine both the direction of the orientation and its prevalence. The preferred orientation was determined in terms of a series of in plane rotation scans around the center of the sample at different tilt or azimuthal angle (see Figure 4.2.1).

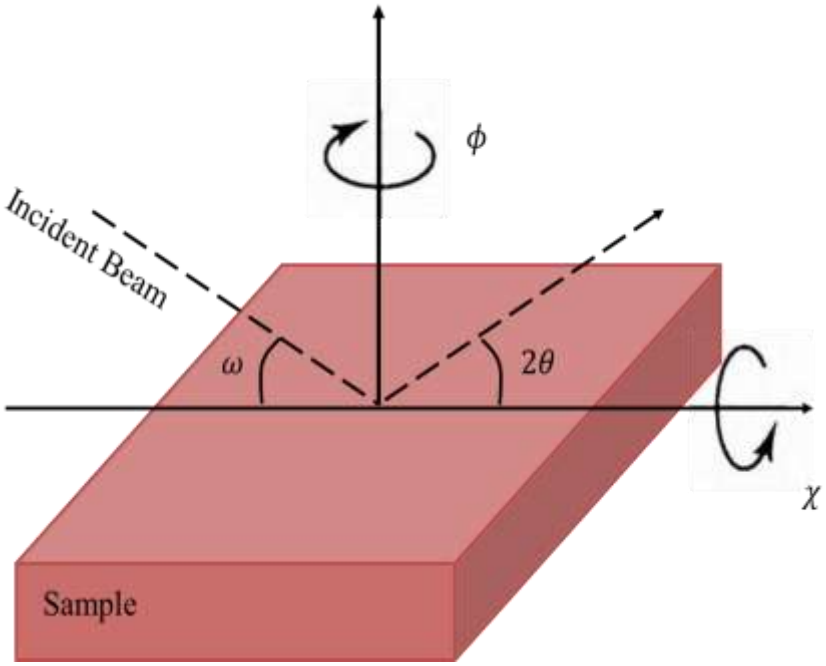

Figure 4.2.1 Experimental set up for XRD-texture measurements at fixed scattering angle $\omega = 2\theta$. The test consists of a series of in plane rotation scans around the center of the sample ϕ at different tilt or azimuthal angle χ, as illustrated.

For the measurements, we used an Empyrean diffractometer from PANalitycal. The variation of diffracted intensity with changing tilt angle χ was recorded using the included X'Pert software. The sample was tilted in $\Delta\chi = 1°$ increments (75° maximum), while ϕ was rotated from 0 to 360° in 1° increments. Results are shown in Figure 4.2.2.

The XRD measurements determine the preferred orientation of the BaM crystallites. Information about the crystallites distribution can be suitable for comparison with magnetization measurements. Also since the recorded intensity is not uniform the crystallites in the sample have a prefer orientation, thus indicating the expected alignment

of the particle during the curing process. This is important since the easy-axis magnetization of BaM follows its crystallite orientation.

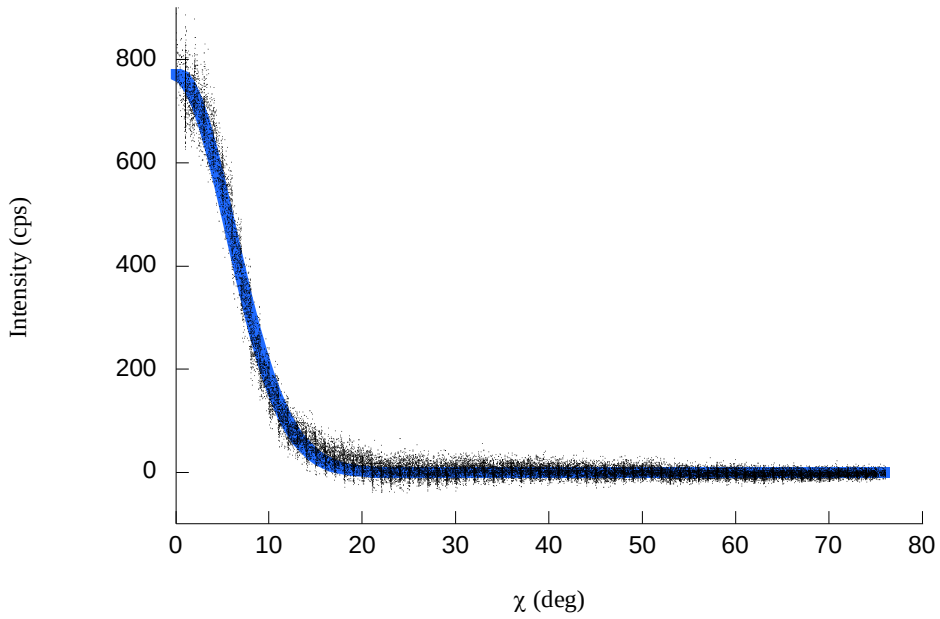

Figure 4.2.2 XRD-texture scan data for every ϕ position, yielding a total of 360 scans per increment of tilt angle χ. Data is well described by a Gaussian curve (thick blue line on the graph). Raw data were corrected for background intensity.

4.3 Results of Analysis of Data Using Distribution Models

To analyze the data, we consider a spherical coordinate system for a set of ferromagnetic particles whose magnetic moments are aligned with an axially symmetric angular ideal distribution $f(\psi)$. The magnetization M of a single particle (Figure 4.3.1) is characterized by two angles, θ and ϕ. The angle θ is defined as the angle the easy axis of the particle makes with the alignment axis (z axis) and ϕ as the rotation projection into

the xy- plane. While the angle ψ is defined as the angle the sample z axis makes with the field.

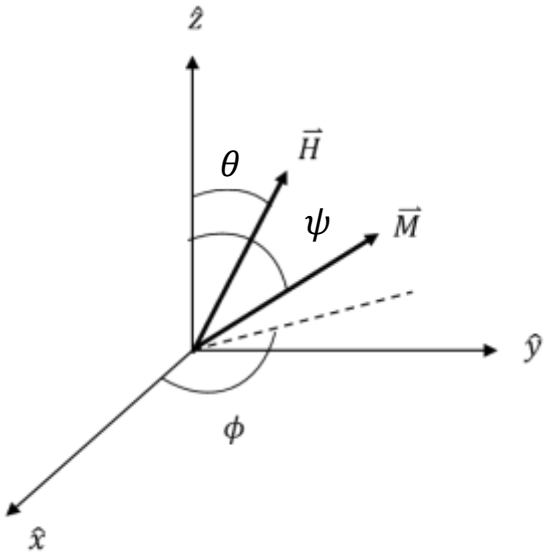

Figure 4.3.1 Illustration of the variables used in the model.

The directions of $\widehat{H}$ and $\widehat{M}$ are

$$\widehat{H} = [\sin\theta]\hat{x} + [\cos\theta]\hat{z} \tag{4.3.1}$$

and

$$\widehat{M} = [\sin\psi\cos\phi]\hat{x} + [\sin\psi\sin\phi]\hat{y} + [\cos\psi]\hat{z} \tag{4.3.2}$$

respectively. Since $\widehat{M} \cdot \widehat{H} \geq 0$ for each individual particle, only the upper half of the sphere is used (i.e. only integrate $0 < \psi < \pi/2$) and the collective average of M for all the particles is expressed by

$$\frac{M(\theta)}{M_s} = \frac{1}{2\pi * N_f} \int_0^{\pi/2} \int_0^{2\pi} f(\psi) \left| \widehat{M} \cdot \widehat{H} \right| \sin\psi \, d\psi d\phi \qquad (4.3.3)$$

where

$$N_f = \int_0^{\pi/2} f(\psi) \sin\psi d\psi \qquad (4.3.4)$$

is the normalization factor.

Figure 4.3.2 shows the results of the expected angular dependence of M_r using the Gaussian distribution found for texture measurements (Figure 4.2.2). The agreement is qualitative at best. However if one includes a 2% randomly oriented component to the distribution (Figure 4.2.2) the data match the calculated values. Note that the 2% random component is below the sensibility of the texture measurements.

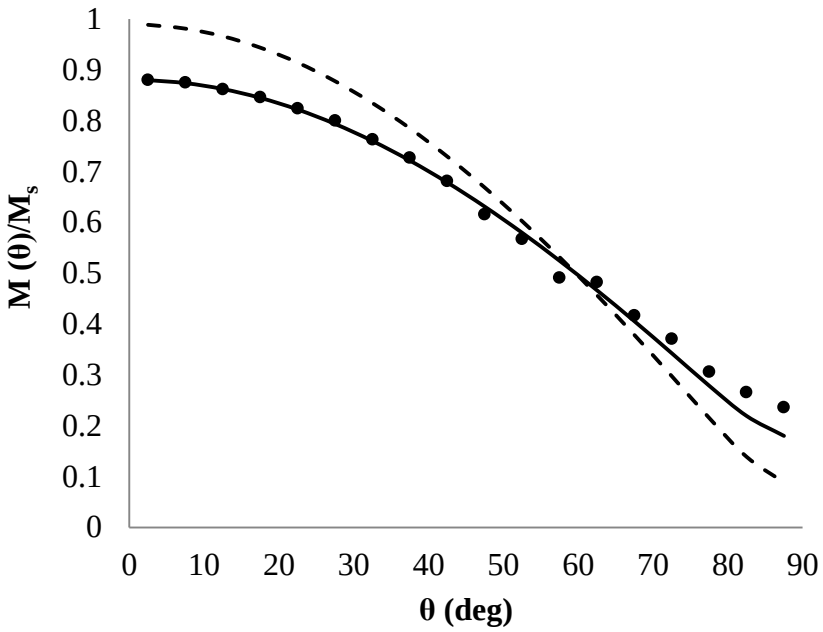

Figure 4.3.2 Modeling of the magnetization orientation in A-H based on remanent magnetization and XRD-texture measurements. The points represent the experimental data. The dashed line represents the Gaussian fit using XRD-texture data and the solid line the same fit plus some small component.

Chapter 5: Modeling Cantilever Bending Behavior

5.1 Motivation and Prior Work

In order to formulate tractable problems in modeling MRE behavior, previous theoretical modeling has been forced to address the issue using simplifying assumptions of material composition and structure, for example roughly spherical soft-magnetic particles either randomly arranged or neatly aligned. This work begins down a computational path, employing simplifying assumptions on behavior that are based on experimentally proven material response, which include both elastic isotropy and magnetic anisotropy. This is an important step since key paradigms of such assumptions, such as the alignment of particles in MREs cured in a magnetic field, are coming under increased scrutiny in MREs with technologically relevant volume fractions and thus are invalidating the basis of previous constitutive models (e.g. Boczkowska [2009], see Chapter 4). A finite element modeling approach allows us to analyze the elasto-magnetic behavior (both kinetic and kinematic) numerically while incorporating experimentally determined elastic and magnetic behavior. The computational method then seeks to solve the problem of determining the combined elasto-magnetic behavior of a given geometry under given external mechanical and magnetic loads.

In this study, we present the simulation of a cantilever beam composed of MRE material (hard- and soft-magnetic) of finite size subjected to a magnetic field. The constitutive equations are based on generalized forms of Hooke's laws and Maxwell's equations for anisotropic materials that depend on the displacement field u and the

magnetic potential vector A as the solution variables. The fundamental problem herein deals with discontinuous changes in physical properties (elastic and magnetic) across interfaces. These physical properties give rise to coupled magnetic and elastic responses that in turn generate forces within an MRE in response to an applied magnetic field and/or external load. These forces are coupled through use of the Maxwell stress tensor which is valuated as a surface traction boundary condition on the cantilever geometry.

The objective of the simulations described in this chapter was to develop predictive simulations of MRE behavior. The objective was pursued by measuring the physical and rheological properties of actual MRE samples and developing continuum elastic and magnetic properties for the MRE particulate composite. The authors use actual magnetization and elastic modulus data from experiments to determine the model's material parameters.

5.1.1 Cantilever Bending Experiment

In a prior work (Von Lockette *et al.* [2010]), a schematic of the blocked-force test setup is shown in Figure 5.1.1. The MRE samples were fixed at the base with 50 mm free length and 20 x 5 mm cross sections. Samples were subjected to increasing magnetic field strengths (up to $\mu_0 H \sim 0.09$T) in order to study the dependence of magnetic field strength and tip deflection on blocking force. Beyond $\mu_0 H \sim 0.09$T the tip of the A-H samples moved beyond the width of the electromagnet's pole faces. Measurements were conducted to determine the amount of force generated at discrete tip displacements of 0,

2.5, 5.1, 7.6, and 10.2 mm, each over the range of field strengths. Displacements were measured with a video microscope with integrated measurement software. Forces were measured with a Shimpo model FGV-0.5x force gauge contacting the tip of the sample via a 254 mm aluminum extension to avoid possible field interference (though none was seen even without the extension).

The measured total load F_T reflected the combined result of the elastic F_e and magnetic F_m responses, i.e.

$$F_T(H) = F_m(H) + F_e \tag{5.1.1}$$

where the magnetic behavior was a function of H. The zero field measurements yielded the elastic forces, $F_T(H = 0) = F_e$, from which the magnetic response $F_m(H)$ was determined.

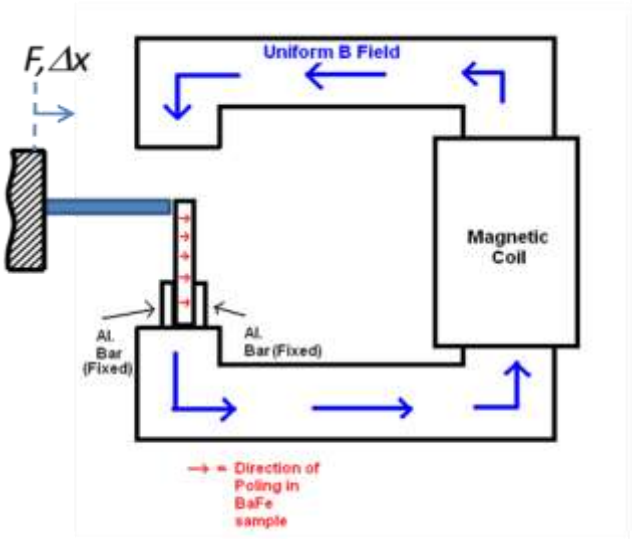

Figure 5.1.1: Experimental Setup of Forced Displacement testing. The force gauge could be moved to give the samples a prescribed displacement.

5.1.2 Results of Cantilever Bending Experiments

5.1.2.1 Elastic Bending Compliance

Results of cantilever bending deflection experiments measuring tip deflection v as a function of $F_T(H)$ were presented in Von Lockette *et al*. [2011]. The data show linear behavior initially for all cases while the A-H and U-H cases show signs of softening at higher deflections. Overall, the A-H and U-H (BaM) samples appear more compliant than the A-S and U-S (Fe) samples. Class U-H and A-H have slopes of 65 and 51 mm/N, respectively, while classes A-S and U-S have slopes of only 33 and 26 mm/N, respectively.

5.1.2.2 Blocked-Force

Blocked-force tests were used to determine the forces exerted by the samples across the same range of proscribed displacements used in the previous experiments but now under the influence of H for $\mu_0 H$ up to 0.09 T.

The most strikingly result, was that the S-MRE material showed $F_m(H) = 0$ zero tip deflection for all field strengths and increasing force with field when displaced to v = 10mm. This is in line with previous observations that Fe-based MREs show no motion in free deflection experiments (Von Lockette *et al.* [2009]). Moreover, it was noticed that the maximum force found in the U-S sample is greater than that found in the A-S material

(0.37N vs. 0.33N, or 11% higher, respectively). This suggests that alignment reduces maximum tip force somewhat but is mitigated by the fact that the U-S sample has lower elastic bending compliance, k, (26 mm/N vs. 33 mm/N, or 27% lower, respectively). In contrast to the aligned A-H sample, the unaligned U-H material shows little to no force under all conditions.

These preceding data are used as the basis for comparison for the FE models developed in this work.

5.2 FEA Model Definition

The problem herein is considered in a 2-D plane as illustrated in Figure 5.2.1.The model consists of two regions: a cantilever beam (Ω) and the surrounding air region (Φ). The dimensions of the beams were length: 50 mm; width: 20 mm; and thickness 5 mm. Basic mechanical and magnetic properties were established from experimental data and literature values: Young's modulus $E_{BaM} = 14$ MPa and $E_{Fe} = 30$ MPa (values which yield accurate bending results), Poisson's ratio $\nu = 0.4$ and density $\rho = 7870$ Kg/m^3 (mixture approximation for the elastomer-composite), and the magnetic saturation of BaM MRE, $M_s = 60$ kA/m (see 3.3 Magnetization Measurements Figure 3.3.1). For Fe the magnetic properties are defined by a measured H-B curve (see 3.3 Magnetization Measurements Figure 3.3.3)

In the air region (simulated as an elastic medium with negligible modulus), the problem solution is governed by electromagnetic behavior. The magnetic field depends on the vector potential $\boldsymbol{A}$ which is determined from the solution to the problem given appropriate boundary conditions in $\boldsymbol{A}$ on 1 and 9 (Figure 5.2.1) and continuity conditions on 4 and 7. The direction of the resulting magnetic field in the air region is then parallel with the y-axis. A moving mesh formulation is used for the calculation of the magnetic field values to account for displacement of the beam relative to the field.

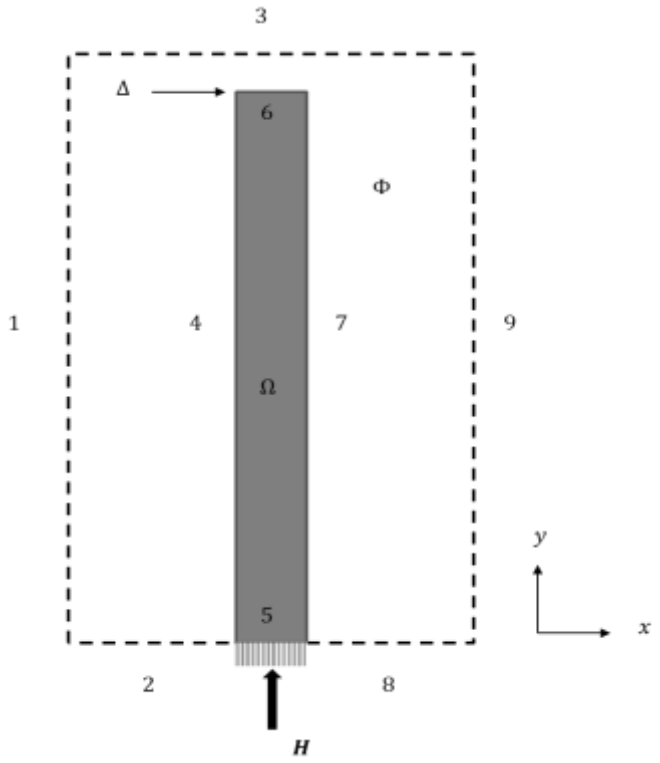

Figure 5.2.1: Geometry of the studied 2-D problem where Ω represents the beam domain in grey, which is fixed at the base and Φ the air domain, dashed line. Boundaries are numbered.

Table 5.2.1: Boundary conditions on the propose model where SC is the surface current, PMC the perfect magnetic conductor, FC the force calculation, BL the boundary load, and PD the prescribe displacement condition.

Boundary Number	**Elastic Boundary Condition**	**Magnetic Boundary Condition**
1	Free	SC (-)
2	Fixed	PMC
3	Free	PMC
4	BL	FC
5	Fixed	FC,PMC
6	PD, BL	FC
7	BL	FC
8	Fixed	PMC
9	Free	SC (+)

The MRE domain Ω is also governed by electromagnetic physics and additionally solid mechanics behavior. The displacement field solution variable $\boldsymbol{u}$ is added to the magnetic vector potential $\boldsymbol{A}$. The base of the MRE sample, boundary 5, is fixed. All four boundaries of the MRE sample, 4, 5, 6, and 7 are subjected to the Maxwell surface stress which relates electromagnetic energy density to linear momentum, here in a static case.

The primary problem COMSOL addresses is the 2-way coupling between the elastic deformation and the magnetic field interactions through the Maxwell stress tensor. As the tip of the beam undergoes blocked or free deformation under the application of a

magnetic field and/or prescribed displacement via applied boundary conditions, a reaction force that tends to bring the beam back to an equilibrium position is created on boundary 6. Hence, the accurate prediction and analysis of this reaction force is important in predicting the actuation capabilities of the MREs. Therefore, the analysis and computation of the x-direction reaction force on boundary 6 (Figure 5.2.1) is of primary interest.

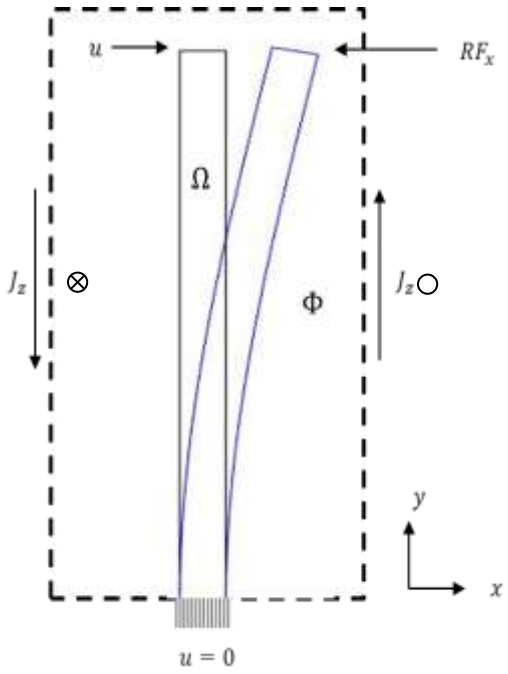

Figure 5.2.2: Schematic of the finite element model showing the direction of: the applied current J_z (the open circle is out and circle with x is into the board), prescribed displacement u, and reaction force RF_x.

5.2.1 Governing Equations

In this, and other works, modeling begins by choosing a magnetic vector potential, $\boldsymbol{A}$, as the independent magnetic variable in the constitutive laws. Relationships between $\boldsymbol{u}$, the independent variable in elasticity theory, and higher order dependent

variable such as strain and stress are employed as well. The elastic and magnetic responses are then coupled through the Maxwell stress tensor. The resulting boundary-value problem can be presented as a set of differential equations coupling elastic and magnetic behavior that can be solved using a finite-element method. To reflect material behavior under combined external mechanical loads and magnetic fields and to come up with a reasonable and applicable magneto-elastic law is still an important issue in linear and nonlinear magneto-elasticity theory.

5.2.1.1 Equations of Elasticity

Herein the magneto-elastic behavior of the MREs is analyzed by an approach in which the appropriate mechanical deformation equations are coupled with electromagnetic equations through the Maxwell stress. Let us consider a differential volume element in static equilibrium within the cantilever beam acted on by an arbitrary body force. A body force is any externally applied force that acts on each element of volume of the continuum, thus, a force per unit volume $\boldsymbol{F}_v$. Applying Newton's first law of motion, we can obtain the set of differential equations that govern the stress σ distribution within the beam,

$$\frac{\partial \sigma_{xx}}{\partial x} + \frac{\partial \sigma_{xy}}{\partial y} + \frac{\partial \sigma_{xz}}{\partial z} + F_x = 0 \qquad (5.1a)$$

$$\frac{\partial \sigma_{xy}}{\partial x} + \frac{\partial \sigma_{yy}}{\partial y} + \frac{\partial \sigma_{yz}}{\partial z} + F_y = 0 \qquad (5.1b)$$

$$\frac{\partial \sigma_{xz}}{\partial x} + \frac{\partial \sigma_{yz}}{\partial y} + \frac{\partial \sigma_{zz}}{\partial z} + F_z = 0 \qquad (5.1c)$$

Since we are interested in the 2D case, it is assumed that $\sigma_{zz} = \sigma_{yz} = \sigma_{xz} = 0$ so that static equilibrium becomes

$$\frac{\partial \sigma_{xx}}{\partial x} + \frac{\partial \sigma_{xy}}{\partial y} + F_x = 0 \qquad (5.2a)$$

$$\frac{\partial \sigma_{xy}}{\partial x} + \frac{\partial \sigma_{yy}}{\partial y} + F_y = 0 \qquad (5.2b)$$

In tensor notation these constitutive equations are given by

$$-\nabla \cdot \boldsymbol{\sigma} = \boldsymbol{F}_v \qquad (5.3)$$

Next we employ generalized Hooke's Law

$$\boldsymbol{\sigma} = \boldsymbol{C\varepsilon} \qquad (5.4)$$

where $\boldsymbol{\sigma}$ is stress tensor, $\boldsymbol{C}$ is the stiffness matrix defined in 2D plane stress by

$$\boldsymbol{C} = \frac{E}{1-v^2}\begin{bmatrix} 1 & v \\ v & 1 \end{bmatrix} \tag{5.5}$$

and $\boldsymbol{\varepsilon}$ is the small strain tensor defined by

$$\boldsymbol{\varepsilon} = \begin{bmatrix} \varepsilon_{xx} & \varepsilon_{xy} \\ \varepsilon_{yx} & \varepsilon_{yy} \end{bmatrix} \tag{5.6}$$

this can be represented in tensor notation as

$$\varepsilon = \frac{1}{2}[(\nabla u)^T + \nabla u] \tag{5.7}$$

Now substituting eqs. (5.5) and (5.6) into (5.4) we can obtain the constitutive equations for a linear elastic material:

$$\varepsilon_{xx} = \frac{1}{E}\left[\sigma_{xx} - v\sigma_{yy}\right] \tag{5.8a}$$

$$\varepsilon_{yy} = \frac{1}{E}\left[v\sigma_{xx} - \sigma_{yy}\right] \tag{5.8b}$$

$$\varepsilon_{xy} = \frac{1+v}{E}\sigma_{xy} \tag{5.8c}$$

Alternately, (5.8a-c) may be inverted to yield:

$$\sigma_{xx} = \frac{E}{(1-\upsilon^2)}\left[\varepsilon_{xx} + \upsilon\varepsilon_{yy}\right] \tag{5.9a}$$

$$\sigma_{yy} = \frac{E}{(1-\upsilon^2)}\left[\upsilon\varepsilon_{xx} + \varepsilon_{yy}\right] \tag{5.9b}$$

$$\sigma_{xy} = \frac{E}{(1+\upsilon)}\varepsilon_{xy} \tag{5.9c}$$

where *E* is Young's modulus, and ν Poisson's ratio, e.g. the component form of eq. (5.4). A final substitution of eqs. (5.9a-c) into (5.3) with no body forces yields the governing equation in terms of the independent displacement variables, u_i,

$$\nabla \cdot \left\{ \boldsymbol{C}\left[\frac{1}{2}\left[(\nabla \boldsymbol{u})^T + \nabla \boldsymbol{u}\right]\right]\right\} = 0 \tag{5.10}$$

These set of equations encompasses what COMSOL solves for the elastic aspect of the elasto-magnetic problem. Though the displacements expected are large, the deformations are not necessarily so. As a first level model we employ the moving mesh and iterative solution capabilities of COMSOL to determine more accurate response at larger deflections using small deformation theory.

5.2.1.2 Equations of Electromagnetism

On the other hand, Maxwell's equations represent the governing equation of electro-magnetic phenomena. In this case,

$$\nabla \times \boldsymbol{E} = -\frac{\partial \boldsymbol{B}}{\partial t} \tag{5.11}$$

$$\nabla \times \boldsymbol{H} = \frac{\partial \boldsymbol{D}}{\partial t} + \boldsymbol{J} \tag{5.12}$$

where $\boldsymbol{E}$ is the electric field intensity, $\boldsymbol{B}$ the magnetic flux density, $\boldsymbol{D}$ the displacement current density, and $\boldsymbol{J}$ the electric current density.

First, we formulate the vector potential $\boldsymbol{A}$ defined by

$$\boldsymbol{B} = \nabla \times \boldsymbol{A} \tag{5.13}$$

Next, assuming a quasistatic model, all time derivatives are zero, specifically

$$\frac{\partial \boldsymbol{B}}{\partial t} = \nabla \times \frac{\partial (\boldsymbol{A})}{\partial t} = 0 \quad \text{and} \quad \frac{\partial \boldsymbol{D}}{\partial t} = 0 \tag{5.14}$$

which, from eq. (5.11) yields

$$\boldsymbol{E} = -\frac{\partial \boldsymbol{A}}{\partial t} = 0 \tag{5.15}$$

Together with the material law,

$$\boldsymbol{J} = \sigma \boldsymbol{E} + \boldsymbol{J_e} \tag{5.16}$$

where σ is the material electric conductivity, $\boldsymbol{J}$ the electric current density, and $\boldsymbol{J_e}$ the applied current density. We can reduce our remaining Maxwell equation to

$$\nabla \times \boldsymbol{H} = \boldsymbol{J_e} \tag{5.17}$$

The three materials in question, the air medium, the Fe-MRE, and the BaM-MRE, have three different $\boldsymbol{B} - \boldsymbol{H}$ relationships**.** The general constitutive equation for the magnetic response of the air medium is given by

$$\boldsymbol{B} = \mu_0 \mu_r \boldsymbol{H} \tag{5.18}$$

yielding the governing equation for the air medium domain in terms of the solution variable, $\boldsymbol{A}$

$$\nabla \times \left(\frac{1}{\mu_0 \, \mu_r} \nabla \times \boldsymbol{A} \right) = \boldsymbol{J_e} \tag{5.19}$$

where μ_r, is the relative permeability of the material (unity in this case) and $\mu_0 = 4\pi x 10^{-7}\ NA^{-2}$ is the permeability of free space.

The general constitutive equation for BaM, a hard magnetic material, can be expressed by

$$\boldsymbol{B} = \mu_0(\boldsymbol{H} + \boldsymbol{M}) \tag{5.20}$$

Therefore, the governing equation for a BaM-MRE domain is given by

$$\nabla \times \left(\frac{1}{\mu_0}\boldsymbol{B} - \boldsymbol{M}\right) = \boldsymbol{J_e} \tag{5.21}$$

which in terms of the solution variable yields

$$\nabla \times \left(\frac{1}{\mu_0}\boldsymbol{\nabla} \times \boldsymbol{A} - \boldsymbol{M}\right) = \boldsymbol{J_e} \tag{5.22}$$

Magnetization values for the anisotropic BaM material were found from experimental results (see 3.3 Magnetization Measurements Figure 3.3.1).

For Fe-MREs the gradual alignment of the magnetic domains within the material causes an increase in $\boldsymbol{B}$ as $\boldsymbol{H}$ is gradually increased. The constitutive relation is not a simple linear function and thus requires a general definition,

$$|\boldsymbol{H}| = f(|\boldsymbol{B}|) \tag{5.23}$$

where the function $f(|\boldsymbol{B}|)$ was from experimental results (see 3.3 Magnetization Measurements Figure 3.3.3). Finally, substituting (5.23) into (5.17) we get

$$\nabla \times f(|\nabla \times \boldsymbol{A}|) = \boldsymbol{J_e} \tag{5.24}$$

5.2.2 Model Boundary Conditions

The basic idea behind our proposed system is to allow the mechanical structure to bend freely (as expected for BaM composites) in the presence of a magnetic field or to impose a tip deflection and measure the required external load via the x-component of the reaction forces. The beam was contained within a simulated air volume modeled as an elastic medium with negligible modulus. The bending results in a nonlinear relationship between the beam tip deflection and the resulting restoring force on its surface.

Prescribed displacements, *u*, are imposed on boundary 6; the resulting restoring force RF_x is determined from reactions at the proscribed displacement boundary. A surface current J_z is applied on both the left and right surfaces of the entire air domain (boundaries 1 and 9). This gives rise to a magnetic field in the *+y* direction, perpendicular to the curing direction, that actuates the cantilevers (see Figure 5.2.1).

A parametric study was developed to determine the influence of the applied magnetic field on the deflection of the beam. Since the applied magnetic field plays a major role in determining the beam deflection, the study defines one parameter: the applied surface current J_z on surface Ω (surface Φ keeps $J_z = 0$) which gives to H and is defined by a start value 0, an end value 1240 A/m, and the step of the range 310 A/m. Then for each prescribe displacement imposed on the tip of the beam, it is possible to calculate the resulting restoring force for a range of magnetic field values and displacements.

5.2.2.1 Mechanical Boundary Conditions (MBCs)

The MBCs are formulated as prescribed displacement $u = u_0$, prescribed constraints where $\boldsymbol{u} = 0$, and boundary load specify on domain Ω. This boundary load is defined by the Maxwell surface stress tensor (included to account for the stress due to the electromagnetic force induced by the magnetic field) on the surface Ω. The calculated Maxwell surface tensor is imposed as a surface traction on the boundary of the MRE (boundaries 4-7) and is the basis of the elasto-magnetic coupling. The Maxwell stress tensor is given by

$$nT = \frac{1}{2}n(H \cdot B) + (n \cdot B)B^T \tag{5.25}$$

where n is the outward normal from the object.

5.2.2.2 Electromagnetic Boundary Conditions (EBCs)

The EBCs are formulated as prescribed surface current $\boldsymbol{J}_{S0}$ (boundaries 1 and 9), perfect magnetic conductor on boundary 5 to impose symmetry for the magnetic field as well as on the upper and lower surfaces of Φ (i.e. boundaries 2,3, and 8) to ensure that the field continued uninterrupted by the end of the air domain.

5.2.3 Mesh Development

Free quadrilateral elements were used to mesh the beam and free triangular elements to mesh the remaining domain. The quality of the triangular mesh was set by the triangulation method: Advancing front. The sizes of the elements were specified by the predefined sizes presented in Table 5.2.3.1. Quadrilateral elements where used to yield more symmetric approximations of the Maxwell surface on the MRE sample's boundaries.

Table 5.2.3.1 Element type and final size of the used mesh.

Domain	**Element**	**Size [mm]**
Beam	Extra Fine	1.6
Air	Extremly Fine	0.8

Determination of an appropriate level of mesh refinement was found from the x-reaction force on boundary 6 as working metric in a mesh-size convergence study. The study started with an extremely coarse divided mesh, which was gradually reduced in size while the *x*-reaction force was tracked. The rate of change between an extremely coarse and coarser mesh was 48.73% at 0.02T. The rate of change between an extremely fine and finer mesh was 27.19% at 0.02T. The rate of change between an extremely fine and an extra fine mesh was 6.35% at 0.02T. Element size reduction was terminated when the results were found to asymptotically converge (see Figure 5.2.3.1). The resulting mesh consisted of 2620 elements and 28340 degrees of freedom (Figure 5.2.3.2.)

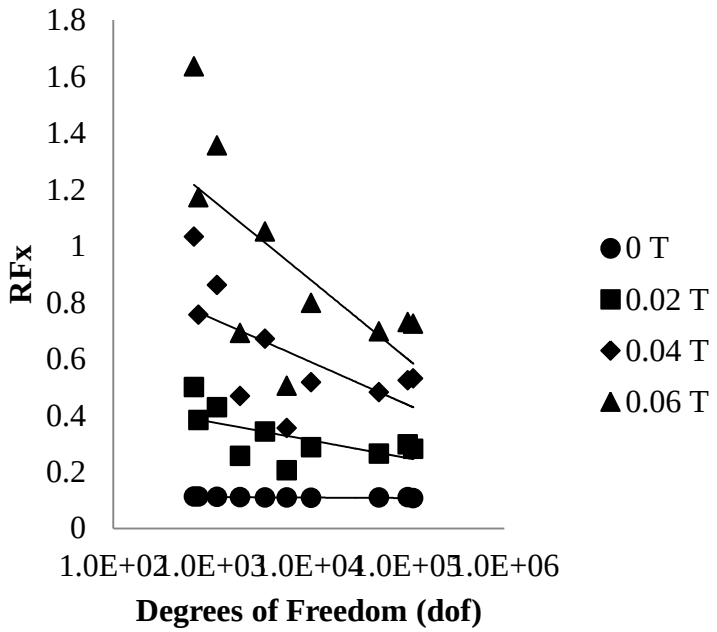

Figure 5.2.3.1: Convergence study of the reaction force *RFx* vs. degrees of freedom (DOF) at specific magnetic field densities.

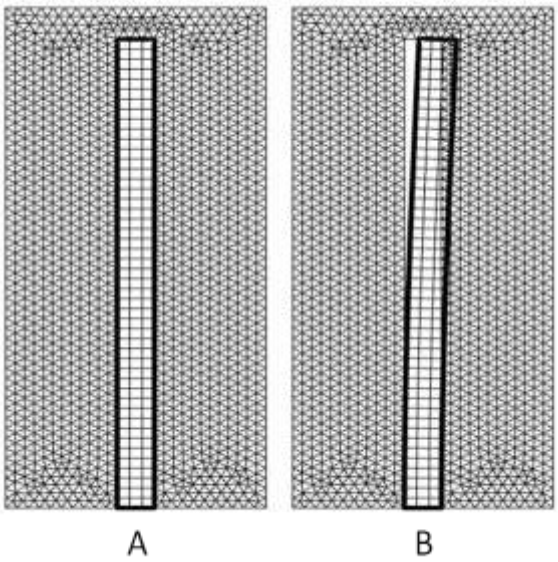

Figure 5.2.3.2 (A) Resulting mesh and (B) 1:1 deformed geometry; the converged mesh consists of 2620 elements and 28340 degrees of freedom. Tip displacement is 4 mm.

5.3 Comparison of Finite Element Model to Experimental Data in Cantilever Bending

In this study, a magneto-elastic finite element formulation was presented. Herein reaction forces to the blocked bending deformation of the beams under the influence of static magnetic field were analyzed using COMSOL. We modeled the blocked-force of an MRE beam either made of nominally 30% v/v 40 micrometer BaM particles, which provides the hard magnetic behavior or 325 mesh Iron (Fe) also at 30% v/v, which serves as a soft magnetic case. Both are combined with a compliant elastomer matrix. The results obtained from the simulation are compared with those reported in the literature and show very good agreement.

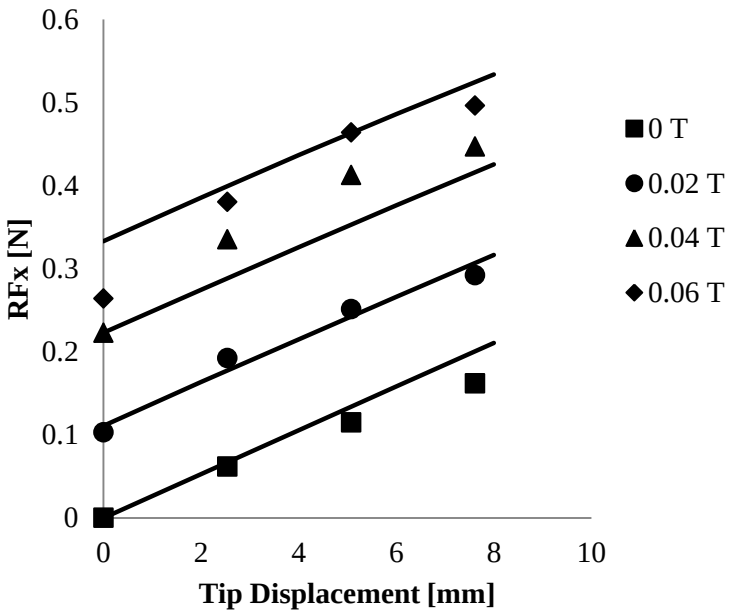

Figure 5.3.1 x-direction reaction force vs. tip displacement for BaM beam MRE composite. Data (in symbols) taken from Von Lockette et al. [2011] is compared to FEM model predictions (lines).

The BaM composite behavior, as reproduced by the simulation, is in very good agreement with experiment on the same material. As shown in Figure 5.3.1, the composite reaction force is non-zero for non-zero field strengths and as expected, they increase with tip deflection and field strength. This result is again in agreement with experimental observation, [Von Lockette 2011]. Nevertheless, in experimental results a non-linear behavior is noticeable as the field is increased and tip displacement increases.

Based on the comparison between the proposed model and experimental data we conclude that the model can be useful to predict the behavior of hard-magnetic MREs especially those comprised of BaM particles. The model could be made more effective if large-deformation and/or hyperelastic material formulations are used. On the contrary,

the Fe composite behavior, as reproduced by the simulation, is not in agreement with experimental data. The author believed that the problem is inherent to the formulation of the Maxwell stress tensor. Once the model becomes asymmetric when it bends, it develops an erroneous net force with +x direction. This error does not go away even at millions of DOF. A suggested fix is to use a virtual work formulation to obtain a solution of the Maxwell tensor that is less dependent on MRE symmetry. However, in the current software one cannot couple this new Maxwell stress solution with the solid mechanics formulation (e.g. assign this traction to the MRE surface). Consequently, the Fe-MRE model is not effective.

Chapter 6: Conclusions and Future Work

6.1 Conclusions

Magnetorheological elastomers (MREs) are materials that consist of magnetically polarizable particles in a non-magnetic medium. Most works examine MREs comprised of carbonyl iron which is both soft magnetic and spherical but in this thesis hard-magnetic particles were studied as well. While performing magnetization measurement in order to validate the fabrication of the four classes we have found some remarkable results, most notably, the remanent magnetization and coercive field values in the A-H class when measured in different directions (parallel and perpendicular) in relation to the poling axis. This clearly suggests a rotation of the ferromagnetic particles in the plane relative to the applied field, behavior which in principle can lead to the development of new devices like sensors and actuators requiring anisotropic magnetization.

Based on the aforementioned findings a distribution model for the interpretation of particle alignments in H-MREs was formulated in order to better understand the orientation of particle magnetizations. We compared orientation measurements taken with VSM and XRD of A-H materials through a distribution model and found that results obtained by both methods are in agreement with our proposed model. While this has been shown before in experimental visualization results, this is the first time it has been shown through magnetization results.

Furthermore, we presented the simulation of a cantilever beam composed of MRE material (hard- and soft-magnetic) of finite size subjected to a magnetic field. We have found that the BaM composite behavior, as reproduced by the simulation, is in very good agreement with experiment on the same material. On the contrary, the Fe composite behavior is not. We believe that the problem is inherent to the formulation of the Maxwell stress tensor in COMSOL. A suggested fix is to use a virtual work formulation to obtain a solution of the Maxwell tensor that is less dependent on MRE symmetry.

We consider that this research project is likely to inspire future studies on the subject both theoretically and experimentally. Furthermore, the techniques used in the present work to define, model, and differentiate the nature of the magnetic torque response can be easily extended and applied to other soft- and hard-MRE systems.

6.2 Proposal for Future Work

Over the course of this work, some important observations were made which will require additional investigation. For a clearer vision of the potentials of MREs in sensor and actuator, further computational analyses should be made. For example development of working Fe actuation simulations are of interest. As stated in Chapter 5 the simulations based on Fe presented herein becomes asymmetric when it bends and develops an erroneous net force with +x direction. A proposed fix for this problem is to use a virtual work formulation and incorporate nonlinear elastic behavior. Furthermore, the working BaM simulations can provide controlled torque through control of an applied magnetic

field. Thus, knowledge of the relationship between the applied current and output torque is required.

In addition to having potential as actuators, MREs can be used to develop sensors for the detection of small magnetic fields. However, there is a need to control the orientation distribution of the particles in order to maximize detection capabilities. Hence, in the future, MREs have to be synthesized such that there will be adequate control over the orientation of the particle magnetization.

At present, works on MREs, theoretical and experimental, have almost exclusively dealt with roughly spherical soft-magnetic filler particles. The use of hard-magnetic particles in herein was a unique contribution to the field. Therefore, experimenting with different ferromagnetic particles, especially hard-magnetic ones, is highly encouraged. There is a great possibility of enhancing the magneto-elastic characteristics of the MREs by examined them as components (e.g. honeycombs, foams, trusses,…) and not just simple geometries for testing.

References

Ausanio, G., *et al*. "Dynamic response limits of an elastic magnet." *Journal of Magnetism and Magnetic Materials*. 290–291 (2005): 836–838.

Bednarek, Stanislaw. "Tensoinductive Effects in Elastic Ferromagnetic Composites." *Chinese Journal of Physics*. 38. (2000): 168-181.

Boczkowska, A., *et al*. "Image analysis of the microstructure of magnetorheological elastomers ." *J Mater Sci*. 44. (2009): 3135–3140.

Borcea, L. and O. Bruno. "On the magneto-elastic properties of elastomer–ferromagnet composites." *Journal of the Mechanics and Physics of Solids.* 49 (2001): 2877-2919.

Castañeda, P. and E. Galipeau. "Homogenization- based constitutive models for magnetorheological elastomers at finite strain." *J.Mech.Phys.Solids*. 59. (2011): 194-215.

Chen, L., *et al*. "Investigation on magnetorheological elastomers based on natural rubber." *J Mater Sci*. 42. (2007): 5483–5489.

Chen, L., X. Gong, and W. Li. "Microstructures and viscoelastic properties of anisotropic magnetorheological elastomer." *Smart Mater. Struct.* 16. (2007): 2645-2650.

Chikasumi, Soshin. *Physics of Ferromagnetism*. 2nd ed. NY: Oxford University Press, 1997.

Coquelle, E., *et al*. "Micromechanical analysis of an elastomer filled with particles organized in chain-like structure." *J Mater Sci*. 41. (2006): 5941-5953.

Davis, L. "Model of magnetorheological elastomers." *Journal of Applied Physics*. 85. (1999): 3348-3351.

Demchuk, S. and V. Kuz'min. "Viscoelastic properties of magnetorheological elastomers in the regime of dynamic deformation." *Journal of Engineering Physics and Thermophysics*. 75. (2002): 396–400.

Dorfmann, A. and R. Ogden. "Magnetoelastic modeling of elastomers." *European Journal of Mechanics A/Solids.* 22. (2003): 497-507.

Dorfmann, A. and R. Ogden. "Nonlinear magnetoelastic deformations of elastomers." *Acta Mechanica*. 167. (2004): 13-28.

Dorfmann, A. and R. Ogden. "Some problems in nonlinear magnetoelasticity." *Z. angew. Math. Phys.* 56. (2005): 718-745.

Ginder, J., *et al*. "Magnetostrictive Phenomena In Magnetorheological Elastomers." *International Journal of Modern Physics B*. 16. (2002): 2412-2418.

Ginder, J., *et al.,* "Magnetorheological elastomers: properties and applications", *SPIE*. 3675. (1999): 131–138.

Gong, X., X. Zhang, and P.Zhang. "Fabrication and characterization of isotropic magnetorheological elastomers." *Polymer Testing*. 24. (2005): 669-676.

Guan, X., X. Dong, and J. Ou. "Magnetostrictive effect of magnetorheological elastomer." *Journal of Magnetism and Magnetic Materials*. 320. (2008): 158-163.

Hu, Y., *et al.* "New magnetorheological elastomers based on polyurethane/Si-rubber hybrid." *Polymer Testing*. 24. (2005): 324–329.

Jiang, W., *et al*. "Enhancement in Magnetorheological Effect of Magnetorheological Elastomers by Surface Modification of Iron Particles." *Chinese Journal of Chemical Physics*. 21. (2008): 87-92.

Jiles, David. *Introduction to Magnetism and Magnetic Materials*. 2nd ed. Chapman & Hall, 1998. 363.

Jolly, M., D. Carlson, and B. Muñoz. "A model of the behavior of magnetorheological materials." *Smart Matter*. Struct.5 (1996): 607-614.

Jolly, M., *et al.*, "The magnetoviscoelastic response of elastomer composites consisting of ferrous particles embedded in polymer matrix", *J. Intel. Mater. Syst. Struct.* 7. (1996): 613–622.

Kankanala, S. and N. Triantafyllidis. "On finitely strained magnetorheological elastomers." *J. Mech. Phys. Solids*. 52. (2004): 2869-2908.

Landau, L.D., and E. M. Lifshitz. *Electrodynamics of Continuous Media*. Oxford: Pergamon Press, 1984.

Lokander, M. and B. Stenberg. "Improving the MR effect in isotropic MR rubber materials" *Polymer Testing.* 22. (2003): 677-680.

Lokander, M. and B. Stenberg. "Performance of isotropic MR rubber materials" *Polymer Testing.* 22. (2003): 245-251.
Ogden, R. *Nonlinear Elastic Deformations*. NY: Wiley & Sons, 1984. 532.

Shen, Y., M. Golnaraghi, and G. Heppler. "Experimental Research and Modeling of Magnetorheological Elastomers." *Journal of Intelligent Material Systems and Structures*. 15. (2004): 27-35.

Shkel, Y. and D. Klingenberg. "Magnetorheology and magnetostriction of isolated chains of nonlinear magnetizable spheres." *J. Rheol.* 45.2 (2001): 351-368.

Shkel, Y. and D. Klingenberg. in *Proceedings of the Seventh International conference on ER Fluids and MR Suspensions*. Edited by R. Tao. World Scientific. Singapore (2000): 252-259.

Steiglitz, K. and L. McBride. "A technique for the identification of linear systems." *IEEE Trans. Autom. Control*. 10. (1965): 461-464.

Tuan, H. and B. Marvalova. "Magnetoelastic anisotropic elastomers in a static magnetic field: Constitutive equations and FEM solutions." *Taylor & Francis Group, London, UK*. (2010).

Varga, Z, G. Filipcsei, and M. Zrınyi. "Magnetic field sensitive functional elastomers with tunable elastic modulus." *Polymer*. 46. (2006): 227–233.

Varga, Z., G. Filipcsei, and M. Zrınyi. "Smart composites with controlled anisotropy." *Polymer*. 46. (2005): 7779–7787.

Von Lockette, P., *et al*. "Dynamic characterization of bimodal particle mixtures in silicone rubber magnetorheological materials." *Polymer Testing*. 27. (2008): 931–935.

Von Lockette, P., *et al.* "Investigating new symmetry classes in magnetorheological elastomers: I. Cantilever bending behavior." *Smart Mater. Struct*. 20. (2011): 105022

Von Lockette, P., *et al.* "Defining and Investigating New Symmetry Classes for the Next Generation of Magnetorheological Elastomers" *Proceedings of the ASME Conference on SMASIS*. (2009): 1310.

Wang, Y., *et al.* "Effects of rubber/magnetic particle interactions on the performance of magnetorheological elastomers." *Polymer Testing*. 25. (2006): 262–267.

Wang, Y., *et al*. "Preparation and Properties of Magnetorheological Elastomers Based on Silicon Rubber/Polystyrene Blend Matrix." *Journal of Applied Polymer Science*. 103. (2007): 3143–3149.

Yin, H., and L. Sun. "Magnetoelasticity of chain-structured ferromagnetic composites." *Applied Physics Letters*. 86. (2005): 261901.

Yin, H., L. Sun, and J. Chen. "Micromechanics-based hyperelastic constitutive modeling of magnetostrictive particle-filled elastomers." *Mechanics of Materials*. 34 (2002): 505-516.

Zhang, X., *et al.,* "Analysis and fabrication of patterned magnetorheological elastomers" *Smart Mater. Struct.* 17. (2008): 045001

Zhou, G. "Complex shear modulus of a magnetorheological elastomer." *Smart Mater. Struct*. 13 (2004): 1203-1210.

Zhou, G. "Shear properties of a magnetorheological elastomer." *Smart Mater. Struct.* 12. (2003): 139-146.

Zhou, G. and J. Li. "Dynamic behavior of a magnetorheological elastomer under uniaxial deformation: I. Experiment." *Smart Mater. Struct.* 12. (2003): 859-872.

Zhou, G. and Z. Jiang. "Deformation in magnetorheological elastomer and elastomer-ferromagnet composite driven by a magnetic field." *Smart Mater. Struct.* 13. (2004): 309-316.